Jagiellonian University
Faculty of Mathematics and Computer Science
Institute of Computer Science and Computer Mathematics

Maciej Manna

Student number: 1065745

Massively Parallel Pseudo-Spectral DNS and LES for Particle-Laden Turbulent Flows under Two-Way Momentum Coupling

Master's Thesis
in COMPUTER SCIENCE

Supervisor:
Dr. hab. Bogdan Rosa
Warsaw University of Life Sciences – SGGW
Institute of Information Technology;
Institute of Meteorology and Water Management
National Research Institute

September 2022

Streszczenie

Przepływy turbulentne z cząstkami fazy rozproszonej zachodzą nieustannie w środowisku naturalnym oraz znajdują liczne zastosowania w procesach przemysłowych. Ważnym tego przykładem są chmury atmosferyczne, które składają się z ogromnej ilości małych kropel wody i kryształków lodu. Wyjaśnienie wzajemnego oddziaływania powietrza (płynu) i aerozolu (cząstek) jest istotne w kontekście poznania mechanizmów rządzących powstawaniem i przebiegiem zjawisk atmosferycznych. Wiedza w tym zakresie jest użyteczna w obszarze meteorologii i służy do opracowywania coraz to bardziej realistycznych modeli powstawania opadu z kropel chmurowych. To z kolei prowadzi do podniesienia dokładności i sprawdzalności numerycznych prognoz pogody. Jednym ze sposobów badania przepływów dyspersyjnych są symulacje numeryczne.

Powszechnie stosowanym do tego celu narzędziem, zapewniającym wysoką dokładność, są tzw. bezpośrednie symulacje numeryczne (direct numerical simulation, DNS). Za pomocą symulacji DNS można pozyskiwać statystyki zderzeniowe cząstek, które to są użyteczne jako parametry w modelach obejmujących większe skale przestrzenne. Symulacje DNS są jednak kosztowne obliczeniowo, co ogranicza ich stosowalność do siatek o średnich rozmiarach ($\sim 2048^3$ węzłów – przy współcześnie dostępnych zasobach obliczeniowych). DNS nie pozwalają modelować turbulencji charakteryzowanej wyższymi liczbami Reynoldsa ($R_\lambda \sim 10^4$), czyli takiej która obserwowana jest w powietrzu atmosferycznym.

Metoda dużych wirów (large-eddy simulation, LES) stanowi alternatywę dla DNS. W tej metodzie drobnoskalowa turbulencja nie jest bezpośrednio rozwiązywana, ale jest parametryzowana przy użyciu modelu podskalowego. Umożliwia to modelowanie przepływów turbulentnych o większej liczbie Reynoldsa przy użyciu siatek o mniejszej liczbie węzłów. Ograniczenie złożoności obliczeniowej odbywa się jednak kosztem mniejszej precyzji i fizycznej dokładności. Niniejsza praca stanowi porównanie obu metod (DNS i LES), zarówno w kwestii fizycznej dokładności, jak i wydajności, skupiając się w szczególności na symulacjach z dwustronnym sprzężeniem pędu pomiędzy płynem i cząstkami. Zostało wykazane, że LES stanowi obiecującą odpowiedź na ograniczenia DNSu, pomimo pewnych niedokładności wynikających z filtrowania turbulencji w najmniejszych skalach. Różnice te, w większości przypadków, stają się mniejsze, gdy uwzględni się dwustronne sprzężenie pędu, w szczególności dla cząstek poddanych działaniu grawitacji.

Przeprowadzone zostały również analizy kosztów obliczeniowych obu metod. Choć zastosowanie LES zapewnia ogromną oszczędność w obliczeniach związanych z turbulentnym przepływem płynu, to jednak koszt ten znacząco rośnie wraz z liczbą cząstek. Niezbędna ilość symulowanych cząstek może zaś być duża, gdyż efekty dwustronnego sprzężenia pędu objawiają się wyraźniej w układach z względnie wysokim stosunkiem masy cząstek i płynu (pomiędzy 0.1 i 1). Obliczenia odnoszące się do dynamiki cząstek stanowią więc bardziej istotne ograniczenie dla LESu niż dla DNSu, gdzie złożoność obliczeń związanych z płynem jest czynnikiem dominującym. Ponadto zidentyfikowano i przeanalizowano szereg parametrów, które pośrednio wpływają na czas trwania symulacji, takie jak np. promienie kropel oraz działanie grawitacji. Na koniec przedstawiono także wpływ preferencyjnego koncentrowania

się cząstek na wariancję ich rozkładu pomiędzy równolegle wykonywanymi procesami. Ten czynnik ma również istotne znaczenie w kontekście całkowitej wydajności symulacji.

Słowa kluczowe

obliczeniowa mechanika płynów, przepływ turbulentny, przepływ wielofazowy, krople, mikrofizyka chmur, obliczenia dużej mocy, równania Naviera-Stokesa, homogeniczna izotropowa turbulencja, statystyki zderzeniowe kropel, metoda pseudo-spektralna, bezpośrednia symulacja numeryczna (DNS), metoda dużych wirów (LES), dwustronne sprzężenie pędu, efekty grawitacyjne

Tytuł pracy w języku polskim

Masywnie równoległe pseudo-spektralne symulacje DNS i LES przepływów turbulentnych z cząstkami przy uwzględnieniu dwustronnego sprzężenia pędu

Abstract

Turbulent fluid flows with dispersed particles are a common occurrence in nature, as well as in many technological processes. An important example of such systems are atmospheric clouds that consist of a huge number of small water droplets and ice crystals suspended in air. The understanding of interplay between air (fluid) and aerosol (particles) is crucial for increasing the accuracy and reliability of numerical weather forecasts through more realistic modelling of atmospheric phenomena. Performing numerical simulations on a fine scale is one way of studying such processes.

Direct numerical simulations (DNS) prove to be a relatively precise tool that is widely used in these studies. DNS can be used to obtain the particle collision statistics obtained from these simulations may be further utilised as parameterisations for larger-scale models. These simulations, however, are costly in terms of computational complexity, hence their application is limited to moderate-sized grids ($\sim 2048^3$ nodes, with the computing power of modern supercomputers). For that reason DNS are not able to resolve turbulence characterised by higher Reynolds numbers ($R_\lambda \sim 10^4$), which is observed in atmospheric air.

Large-eddy simulations (LES) provide an alternative approach to DNS. In this method small-scale turbulence is not directly resolved but parameterised using a subgrid-scale model. This reduces the grid size required to achieve higher Reynolds numbers (and, thus, computational complexity) at the cost of diminished precision and physical fidelity. This thesis provides comparison of DNS and LES, both in terms of physical fidelity and performance, focusing primarily on simulations under two-way momentum coupling between the fluid and particles. LES is shown to be a promising solution to limitations of DNS, even though it exhibits certain inaccuracies that may be attributed to the filtering of small-scale vortical structures. These discrepancies, for the most part, become less pronounced when two-way momentum coupling is considered, especially for settling particles.

Furthermore, a broader study of computational costs for both methods is presented. Even though LES provides immense performance advantage when it comes to fluid simulation, it is highly susceptible to the growing number of individually tracked particles. The amount of particles that are needed may be considerable, as effects of two-way momentum coupling manifest when particle mass loadings are relatively high (between 0.1 and 1). Thus, computations related to particles are recognised to be a much more significant bottleneck for LES than for DNS, where the complexity of fluid simulation is the largest concern. In addition, several parameters that indirectly influence the execution time are identified and analysed, such as droplet radii or effects of gravity. Finally, it is shown that the preferential concentration of particles may affect the variance of their distribution between parallel processes and consequently influence the overall simulation performance.

Keywords

Contents

Acknowledgements

Introduction

Turbulence is the phenomenon that accompanies most of the real-world situations where fluid flows are encountered. Distinction between laminar and turbulent flows is very practical, as the former represents much more organised, layered, and stable fluid motion that is easier to analyse and quantify, while the latter is inherently irregular, and its parameters have to be approached statistically. Turbulence gives rise to eddies that span wide range of spatial and temporal scales where different dynamical properties of the fluid are most pronounced. We commonly distinguish three subranges in the entire span of eddy sizes. There is integral length scale that includes largest eddies containing most of the energy of a system. Then, we consider inertial subrange, where turbulence kinetic energy is transferred from larger eddies to the smaller ones in a process referred to as the energy cascade. Finally, we have subrange that consists of smallest eddy sizes, the so-called Kolmogorov microscale, where influence of fluid viscosity is paramount, and where the kinetic energy of slowly vanishing eddies is dissipated into heat. Such complex behaviour arises due to the nonlinearity of equations governing the fluid motion, which makes turbulent flows famously difficult to study analytically. Hence, numeric simulations are often employed to model and study these physical phenomena.

Many processes that involve fluid flows, whether laminar or turbulent, are composed of more than one phase. Here, by phase, we understand regions of the system with the same properties that can be clearly separated by some interface from others. We refer to such flows as multi-phase, or two-phase, in a common case where the number of considered phases is limited to two. These phases often are of different states of matter, e.g. gas–liquid for air bubbles flowing in the water pipe, but systems with two immiscible liquids, such as water and crude oil in pipelines, are also studied (Brauner 2003). In many cases, one of the phases may be treated as continuous (referred to as the continuous phase, or the carrier fluid), while the other remains in separated chunks. We refer to such chunks as the disperse phase, and examples may include air bubbles, water droplets, solid particulate matter suspended in a fluid, etc. Often enough, elements of disperse phase may be approximated as point particles, i.e. material points that are conceptually representing small spheres of given radii, that are considered insoluble and immiscible (that is, they cannot exchange mass with the carrier fluid, suddenly appear, or be destroyed). Such approximation is especially accurate when disperse phase consists of small droplets or bubbles of one fluid surrounded by another, as the surface tension naturally preserves spherical shape of disperse elements. Cloud droplets, in particular, remain spherical since the capillary pressure is several orders of magnitude larger than the local fluid shear stress induced by the disturbance flow associated with their motion. Furthermore, Balachandar and Eaton (2010, Figure 1, therein) point out that for such approximation to be valid, particle response times have to be greater than Kolmogorov time scale of background turbulent flow. We shall refer to two-phase flows with disperse phase approximated by point particles as particle-laden.

The modelling of flows that both exhibit turbulent behaviour and include population of particles interacting with that flow gives rise to even more complexity. As stated by Bal-

achandar and Eaton (2010), "turbulence and multiphase flows are two of the most challenging topics in fluid mechanics, and when combined they pose a formidable challenge, even in the dilute dispersed regime". In spite of that, the number and importance of real-life applications that involve such systems is quite significant, and more than justifies development of effective methods in that domain. To mention just a few, we may consider some technological, and industrial applications, such as analysis of combustion of liquid fuel aerosols in engines, or combustion of pulverised coal in furnaces (Zheng et al. 2020), as well as other technologies, including fluidised beds, transport systems, and pollution control (Crowe et al. 2012, pp. 4–17). Such systems are also studied in ecology (e.g. transport of pollutants in the atmosphere or sediments in water) and agriculture (efficient spraying of fertilisers). Finally, the modelling of atmospheric clouds, that essentially are huge collections of small water droplets and ice crystals suspended in often turbulent air, is the backbone of all meteorological and climate science models used for analysis and prediction (Devenish et al. 2012; Grabowski and Wang 2013). In this thesis we shall focus our study of particle-laden turbulent flows on applications in cloud modelling, but general methods presented here are not limited to that particular use case.

The modelling of atmospheric clouds is a broad domain that has to deal with wide range of length scales, where different structures and physical processes are important and have to be directly represented, while others need to be parameterised due to constraints in computing power. Such tradeoff between computational complexity and physical fidelity of simulations gives rise to the plethora of methods used depending on the respective scale. Simplified picture of that situation is presented in Figure 1. At the largest scales we have global climate models (GCM) and global weather models (GWM, e.g. Integrated Forecasting System, Global Forecasting Systems, ICON), where computation domain often spans the entire Earth ($\sim 10^7$ m) and each cell has (horizontal) dimensions ranging from 10 to 100 kilometres. We also consider mesoscale models that are mainly used for weather prediction in smaller domains that usually cover regions, countries, or continents ($\sim 10^5$–10^6 m) and grid spacing is in the order of kilometres. For instance, maximal resolution of mesoscale model COSMO used for weather forecasting in Poland is 2.8 km (Doms and Baldauf 2021). In this context it is worth adding that a small cloud with a volume of 1 km^3 may contain 10^{17} or more droplets. Both types of models, due to relatively large grid cell sizes, cannot fully resolve even fairly large cloud structures and depend on a lot of parameterisations. In the middle ground, we have cloud resolving models (CRM; domain sizes—kilometres, cell sizes—metres) that cannot fully resolve all turbulent scales of air or exactly model behaviour of every droplet, thus necessary parameterisations are employed, such as large-eddy simulations (LES) and super-droplet method (Arabas and Shima 2013). CRM is commonly employed for research studies focused on the effects of microphysical processes affecting entire clouds, their formation and evolution, precipitation, etc. For that reason, CRMs are used to refine cloud parameterisations used in GCM and mesoscale models.

Finally, we enter scales where point-particle direct numerical simulations (DNS) can be used to obtain more precise picture of small-scale turbulent phenomena that affect cloud microphysics. These methods allow direct resolution of wide range of turbulent scales, including Kolmogorov microscales, which are estimated to be of the order of 1 mm in Earth's atmosphere. Also, all particles (droplets) are individually tracked, so that their dynamics and interaction with carrier flow may be directly computed (note, that 1 m^3 of cloudy volume contains, approximately, up to 10^8 droplets). Due to fine sizes of grid cells required to resolve even the smallest eddies, as well as considerable computational demand of handling large numbers of particles, point-particle DNS are limited to volumes of about 1 m^3 (Morrison et al. 2020).
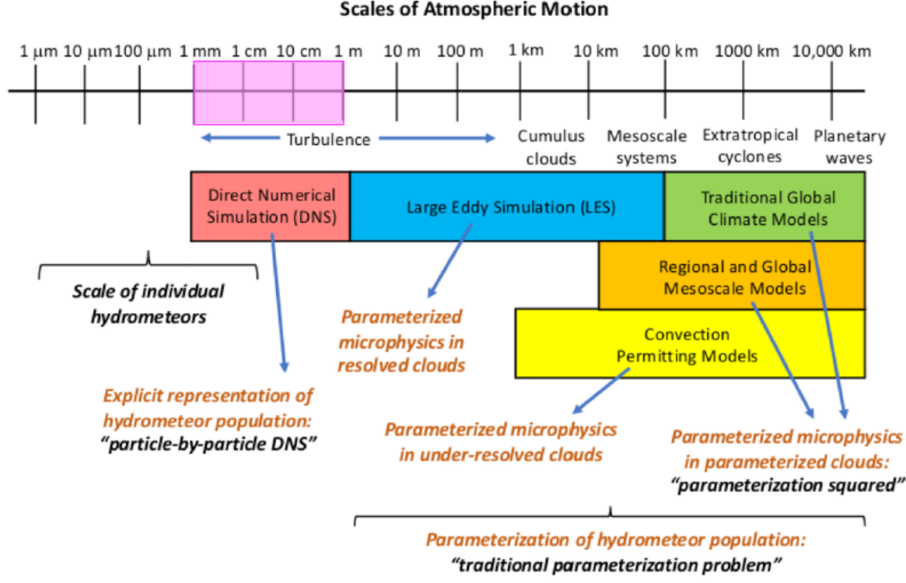
Scales of Atmospheric Motion

Figure 1: Hierarchy of atmospheric models and the scales of atmospheric motion reproduced from Morrison et al. (2020) with author's permission. Coloured rectangles represent types of simulations commonly used when working with respective length scales, and comments emphasise transition from directly resolving most elements of the model (left) to including more and more parameterisations with the increase of scale (right). Magenta rectangle positioned on the axis was added to emphasise range of scales that corresponds to simulations discussed in this thesis.

Despite these limitations, however, such simulations provide essential backbone to entire hierarchy of models by allowing to study small-scale cloud phenomena and estimate parameters used in cloud resolving models (CRM). One example of such parameter is the collision kernel that determines rates of collision between droplets of the same or different sizes, and it greatly affects process of droplet growth due to coalescence that is crucial for accurate modelling of precipitation. Such small domains also justify modelling air turbulence as homogeneous and isotropic. Even though energy-containing large-scale eddies in atmosphere generate large-scale inhomogeneity and anisotropy, dissipative small-scale eddies work to flatten the inhomogeneities, leading to local homogeneity and isotropy. This local homogeneity assumption is the basis of most turbulence models (Matsuda et al. 2021).

There is, however, another important axis which exhibits similar complexity–fidelity tradeoff, and it pertains to the precision of modelling interactions between particles and carrier fluid. We use Lagrangian approach to track particles, since time microscales associated with the energy dissipation of atmospheric flows and response times of cloud droplets are usually of the same order (i.e. the Stokes number, St, is close to 1, see Balachandar 2009). The modelling of interaction between fluid and particles, however, may be limited to one-way momentum coupling (OWC). It means that particles are transported by the fluid but do not affect its velocity field. This simplification is valid for dilute systems, where ratio of total mass of particles to total mass of fluid (referred to as the particle mass loading, Φ_m, of the system) is small, usually assumed to be less than 0.1 (i.e. less than 0.01% by volume for water droplets in air). Despite that, experiments have shown that presence of particles alters statistics of the carrier fluid flow, e.g. suppresses or enhances the turbulence flow depending on the sizes of particles (Gore and Crowe 1989). Also, recent simulation studies (Rosa et al. 2020) have shown that inclusion of momentum transfer in the other direction,

i.e. two-way momentum coupling (TWC), provides a more complete and complex picture of system dynamics, and increase physical fidelity of obtained results, even for relatively dilute systems. Hence, TWC approach is used here, building upon methods and results from Rosa et al. (2020, 2022). Note, that for very dense systems ($\Phi_m > 1$) it is preferable to also include effects of collisions between particles (four-way momentum coupling), but such conditions are not applicable when considering Earth's atmospheric clouds. Also, in this context, it is worth to mention alternative methods for modelling interactions between particles, such as simplified representation of many-body aerodynamic interactions (Hybrid DNS, see Ayala et al. 2007; Wang et al. 2009) or inclusion of lubrication forces (Ababaei et al. 2021), however these approaches are beyond the scope of this study.

In this thesis, small-scale simulations of turbulent, particle-laden flows are considered for the purpose of obtaining particle collision statistics, such as previously mentioned collision kernels. The domain in question is small enough that we can employ direct numerical simulations for the modelling of homogeneous isotropic turbulence (HIT). For simplicity, the domain is assumed to be box-shaped and uniformly divided into cubic cells in all three dimensions. Also, periodic boundary conditions are imposed on the domain walls. As introduced above, the default method applicable for such experiments is point-particle DNS.

Recent studies, however, have shown that direct numerical simulations are close to their limits due to prohibitively large computational costs. Rosa et al. (2013, 2016) used grids of up to 1024^3 nodes, which seems to be the reasonable limit for most studies, although there were studies using even larger grids—e.g. 2048^3 nodes in Ireland et al. (2016) and Matsuda et al. (2021); for flows without particles grids of size 8192^3 were used (Buaria et al. 2019) and more recently even up to $12\,288^3$ (Buaria et al. 2020). It is important to note that grid size is crucial for turbulent flow simulations since it affects the range of spatial scales that can be resolved—from the smallest eddies with sizes close to the spatial grid spacing, to the largest ones of sizes typically about $1/3$ of the computational domain (this limitation is due to a numerical requirement that the correlation of fluid velocity at distances comparable to the domain size must vanish). Such range between largest and smallest resolvable scales can be expressed using Reynolds numbe, which is commonly interpreted as a measure of magnitude of turbuence. Examples of values of the Taylor microscale (that is, considering only eddies in inertial subrange) Reynolds number, R_λ, attained in previous high-resolution studies are $R_\lambda = 499$ for 1024^3 grid (Rosa et al. 2013, 2016); $R_\lambda = 597$ (Ireland et al. 2016), and $R_\lambda = 531$ (Matsuda et al. 2021) for 2048^3 grids; $R_\lambda = 650$ for 8192^3 (Buaria et al. 2019); and $R_\lambda = 1300$ for $12\,288^3$ grid. It is desirable, however, to attain higher values of R_λ to simulate conditions that are present in typical atmospheric clouds, where R_λ is known to attain values between 10^3 and 10^4. What is more, the increase of the Taylor microscale Reynolds number with the number of grid nodes in one dimension, N, is sublinear (comparison of simulation data from various studies shows that $R_\lambda \propto N^{2/3}$, see Wang et al. 2009, Figure 1 therein, which agrees with theoretical estimates for pseudo-spectral method in Pope 2000, Equation 9.8 therein). Thus, when we double N we only increase R_λ by at most 50%–60%, while total number of grid nodes, N^3, increases by the factor of 8. The strategy of increasing grid sizes of DNS to model somewhat wider range of turbulent scales currently faces not only resource limitations, but is also hindered by the diminishing returns in the long run. This situation calls for an alternative solution.

Large-eddy simulation (LES) is a well-developed method that is commonly used when dealing with length scales specific to CRM simulations (Guichard and Couvreux 2017). Its purpose is to allow modelling of highly turbulent environments in larger domains, where directly resolving smallest eddies is infeasible. The general idea is to directly resolve larger

eddies, as in DNS, but replace the direct resolution of the smallest, dissipative turbulent scales with parameterised model, referred to as the subgrid-scale model. This way smaller grid sizes may be used to obtain statistics of turbulent flow that are comparable to DNS, including the Reynolds number.

LES focuses on directly resolving larger scales of turbulence since they contain most of the energy of the system, and are most effective transporters of conserved properties (Ferziger et al. 2020, p. 367; Pope 2000, p. 352). This property is paramount for CRM, but when using simulations to study small-scale phenomena such strategy is not as easily transferable. Also, it was repeatedly shown that relative motion and preferential concentration of low-inertia particles is governed mainly by small turbulent structures. Consequently, the collision-coalescence depends on scales of motion that belong to the dissipation subrange of the energy spectrum. The interest in applying LES method in small-scale experiments used to estimate particle statistics may be limited, but is growing in recent decades (Fede and Simonin 2006; Jin et al. 2010; Rosa and Pozorski 2017), but no comparable studies that also include effects of TWC were performed. Therefore, it is called for to investigate feasibility of LES in that context, and this thesis aims at providing good starting point for such analyses.

The first systematic study using DNS of homogeneous and isotropic turbulence with non-settling particles (i.e. unaffected by gravity) under two-way momentum coupling was performed more than thirty years ago by Squires and Eaton (1990). It focused on the effects that particles have on carrier flow, especially the modulation of turbulence and changes in energy and dissipation spectra due to varying particle mass loadings. Their simulations, due to contemporaneous hardware limitations, used small grid sizes (32^3 and 64^3) and thus were limited to $R_\lambda = 38$. In a follow-up study by Elghobashi and Truesdell (1993) the effect of gravitational settling was considered but the simulations were limited to decaying turbulence. Other early studies, such as Wang and Maxey (1993) and Yang and Lei (1998), expanded these results to larger meshes but were limited to the one-way momentum coupling. More importantly, the latter study (Yang and Lei 1998) proposed to use LES to achieve higher R_λ without going beyond hardware limitations.

These earlier studies, however, did not explicitly consider collisional statistics of particles, such as collision kernels, which are main focus of this thesis. One of the first systematic studies aimed at estimating these parameters using DNS with homogeneous isotropic turbulence model was Ayala et al. (2008), and it was motivated by growing interest in the process of droplet growth due to collision-coalescence. Their simulations included effects of gravity and were performed at different values of the energy dissipation rate. In another study by Wang et al. (2008) the main focus was also on collision statistics, but also hydrodynamic interaction between droplets was considered by employing an original method elaborated by Ayala et al. (2007). In both cases, no influence of particles on the fluid flow was taken into account (as in TWC), but their method attempted to model hydrodynamic interactions between particles instead. An example of earlier TWC study that focused on particle statistics may be the work of Bosse et al. (2006), that shows significant enhancement in the mean settling velocity when two-way coupling is considered. Later, these results were extended by Monchaux and Dejoan (2017) for wider ranges of particle volume loadings, also reporting decrease in particle preferential concentration with increasing mass loading.

Two important features of further studies, at least from the point of view of this thesis, are: (1) inclusion of two-way momentum coupling between fluid and particles, and (2) use of large-eddy simulations in that context. Most of these, however, used only direct numerical simulations that were limited to one-way momentum coupling. Rosa et al. (2013) provides results from simulations spanning wide range of grid sizes (from $N = 32$ to $N = 1024$),

and shows, in practice, diminishing growth of R_λ with respect to N. It also analysed the influence of different forcing schemes on the estimated particle statistics. Further studies by Onishi et al. (2013) and Ireland et al. (2016) are notable because of relatively large grids used that allowed to obtain higher values of R_λ ($N = 2048$ with $R_\lambda = 597$, and $N = 2000$ with $R_\lambda = 527$, respectively). Work by Onishi et al. (2013) is also worth mentioning, as instead of pseudo-spectral method it uses finite-difference method, which is considered to be easier to parallelise and adapt to multiprocessor machines. On that note, of some interest are also recent papers that use Lattice Boltzmann Method to solve underlying homogeneous and isotropic turbulent flow populated by particles tracked using Lagrangian approach (Ernst et al. 2019; Lain et al. 2020). These studies, however, used only grids of size 128^3 and since working with highly turbulent flows was not their main goal they were limited to $R_\lambda = 20$. More recent study of Matsuda et al. (2021) is notable for used grid sizes (up to 2048^3) and impressive number of particles tracked (up to 1 billion), as well as interesting measurements of scale-dependent flatness and skewness of particle distribution fields based on wavelets. Still, these experiments were limited to one-way momentum coupling.

Nonetheless, as already mentioned, it was recent study of Rosa et al. (2020) that systematically analysed the effects of including two-way momentum coupling on basic statistics of the carrier flow, as well as collision statistics of particles. Their results show that using TWC significantly affects particle statistics that measure clustering, radial relative velocities, and collision rates, as well as dependence of these statistics on the particle mass loading. These results were recently complemented by Rosa et al. (2022), where simulations covering broader range of grid sizes were performed (up to 1024^3), and the influence of TWC on average settling velocity of particles was explored as well. Still, both of those studies were limited to DNS method only.

On the other hand, first systematic study of using LES method for simulating steady homogeneous isotropic turbulence for carrier fluid in particle-laden systems was performed by Fede and Simonin (2006). Simulations were performed using finite-volume method on grids with 128^3 nodes. Their effort was focused on measuring influence of subgid-scale modelling on the behaviour of heavy inertial particles at collision distances. In particular, they established that using LES significantly affects particle concentration and collision statistics, as they depend on small-scale motion of carrier fluid. Their analysis was limited to non-settling particles. Marchioli et al. (2008) arrived at similar conclusions, i.e. that filtering velocity field at small-scales leads to inaccuracies in representation of particle segregation and accumulation phenomena in simulations involving wall-bounded flows. Meanwhile, Yang et al. (2008) showed that for different particle statistics, such as longtime single-particle dispersion, some effects of LES parameterisation cancel each other, leading to accurate predictions. More in depth study on the influence of subgrid-scale modelling on preferential concentration of particles, where principal requirements for such models were established, was proposed by Pozorski and Apte (2009).

Important comprehensive study of impact of subgrid-scale modelling on particle collision statistics in HIT was performed by Jin et al. (2010). They used the pseudo-spectral method for the fluid flow calculations and their realisation of LES (i.e. using spectral eddy viscosity model) matches numerical method used in this thesis. Their results confirmed adverse effect of LES on the accuracy of particle-pair statistics, as well as established relation between Stokes number, St, and sensitivity of these statistics to subgrid-scale modelling. They concluded that such effects are most noticeable when $St < 3$. This study involved only non-settling particles. It was later complemented by Rosa and Pozorski (2017) that used the same numerical setup but focused on particles affected by gravity. Their results confirmed previous conclusions regarding limitations of LES to properly represent collisional statistics,

such as radial distribution function and radial relative velocity. They also established influence of subgrid-scale modelling on seemingly single-particle statistics, such as average settling velocity. All studies mentioned above were limited to one-way momentum coupling.

The natural continuation of aforementioned studies is to analyse the influence of both such extensions applied together in the same simulations. Thus, more precisely, the topic of this thesis regards simulations of homogeneous isotropic turbulence with inertial particles under two-way momentum coupling, both with and without effects of gravity, for the purpose of estimating their collisional statistics. Also effects of particles on basic flow statistics shall be discussed. Both direct numerical simulations (DNS) and large-eddy simulations (LES) are used to obtain results, providing grounds for comparison of both methods. To the knowledge of the author, it is the first study in this context, where TWC LES simulations are considered. For the sake of simplicity, all simulations performed as part of this study will use single, moderately-sized grid of 256^3 nodes for DNS, and 64^3 for LES, as in Jin et al. (2010) and Rosa and Pozorski (2017). This study aims to fit into much broader and pressing issue of computational limits that are faced by DNS and establishment of LES as an alternative that opens way to more faithful modelling of atmospheric turbulence.

The comparison between DNS and LES is carried out in two following aspects.

Firstly, the accuracy, or physical fidelity, of LES is analysed. Establishing exact measures of accuracy for collisional statistics is a challenging task because of experimental constraints, as simultaneous measurement of positions and velocities of large amounts of small droplets faces technical limitations, although considerable advances have been made recently in that field (Yavuz et al. 2018). Moreover, homogeneous and isotropic model of turbulence is an idealisation that could not be exactly replicated in actual physical conditions. For these reasons it is difficult to obtain experimental results for validation, and due to the complexity of the problem at hand, no analytical solutions are available as well. On the other hand, difficulties in obtaining experimental data makes estimations of these statistics *in silico* even more valuable. Thus, as in previous studies, the accuracy comparison will mostly focus on qualitative and quantitative differences between results obtained by DNS and LES. The results of DNS are used as a baseline, under the assumption that this method is thoroughly studied and frequently used, and thus provides accurate estimates of parameters in question. Hence, results obtained using LES are compared against them, in order to consider feasibility of LES as a workable replacement for DNS. The further analysis will focus mainly on simulations under two-way momentum coupling.

Secondly, the performance of these two methods will be compared. The main advantage of LES is its reduced computational cost while attaining similar values of R_λ. Such claim needs to be thoroughly verified, especially when simulations with particle-laden flows are considered, where computational load not only scales with grid size used to resolve fluid flow but also with the number of individually tracked particles. That impact is not easy to predict as computations concerning both phases are performed side-by-side in a massively parallel context. Thus, a series of experiments will be performed to establish possible performance gains provided by LES and whether they can be easily achieved by using the same code architecture and parallelisation strategy as for DNS.

The organisation of this thesis directly follows goals and aspects of analysis outlined above. The entire text is divided into three chapters. The first one consists of brief explanation of the numerical method underlining all simulations used to obtain results presented thereafter. The emphasis is placed on the pseudo-spectral method used for fluid flow simulation, difference between DNS and LES methods, and modelling of interactions between fluid and particles. In addition, some information on implementation details is given. Second chapter introduces

relevant flow and particle statistics that are being estimated in simulations. More importantly, the results of simulations will be presented and analysed here in order to compare the physical fidelity and feasibility of LES vs DNS. Results related to modelling under one-way momentum coupling will be recreated, and validated with respect to previous studies. Then, results that include the effect of two-way coupling will be presented for both DNS and LES, depending on particle radii, as well as particle mass loading. In the last chapter, results of performance comparison between DNS and LES shall be presented and discussed. These will focus on simulation wall-clock times depending on the various parameters of simulations, in order to estimate their influence on the computational cost of the solver code. Also, more in-depth profiling data shall be presented, as well as analysis of particle distribution in computational subdomains and its impact on the performance of both methods.

Chapter 1

Numerical Methods

The challenges of numerical modelling of particle-laden turbulent flows are manifold and are mainly associated with the need to keep track of evolution of two distinct phases—continuous fluid flow and discrete particles—as well as their interactions. In this study, the standard Eulerian-Lagrangian approach is used. It introduces two different representations for two phases: velocity field of turbulent flow is evaluated on the nodes of a fixed grid, while each particle has its current position and velocity individually tracked. Moreover, two different methods of simulating fluid flow are employed: direct numerical simulations (DNS) and large-eddy simulations (LES), both within the base framework of the pseudo-spectral method. Finally, beyond conceptual and numerical issues, such multiphase systems prove difficult to be effectively implemented for a massively parallel computing environments (supercomputers) and it will be addressed in the last section.

1.1. Fluid Flow Simulation with Pseudo-Spectral Method

The time evolution of turbulent fluid flow for simulations presented here is performed on the three-dimensional uniform cubical mesh with N equally spaced grid points in each spatial dimension (see Figure 1.2). For this study, the domain size (for DNS) was set to $N = 256$, for the total of $256^3 \approx 16.8$ million grid points. The values of three-dimensional fluid velocity field $\mathbf{U}(\mathbf{x}, t)$ are evaluated at each time step and spatial grid point according to time-dependent Navier-Stokes equations for incompressible flows, as presented below in rotational form

$$\begin{cases} \frac{\partial \mathbf{U}}{\partial t} = -\mathbf{U} \times \boldsymbol{\omega} - \nabla \left(\frac{P}{\rho} + \frac{1}{2}\mathbf{U}^2 \right) + \nu \nabla^2 \mathbf{U} + \mathbf{f} + \mathbf{f}^{(p)} \\ \nabla \cdot \mathbf{U} = 0 \end{cases} \tag{1.1}$$

where: $\boldsymbol{\omega} = \nabla \times \mathbf{U}$ denotes vorticity, P – pressure, ρ – fluid density, and ν – kinematic viscosity of the fluid. Other contributions come from large-scale force, $\mathbf{f}$, used to achieve and maintain the statistically stationary state of homogeneous isotropic turbulence, together with the cumulative force exerted by particles on fluid per unit mass, $\mathbf{f}^{(p)}$, which is non-zero for simulations under two-way momentum coupling (TWC) where effects of particles on the fluid flow are considered (see Section 1.3). Due to idealised nature of considered system, we may assume periodic boundary conditions in all three spatial directions.

   The numerical integration of the Navier-Stokes equations is performed using the -spectral method which is well-established for such simulations. It was first introduced by Orszag and Patterson (1972) and later developed with parallel execution in mind and for application to particle-laden flows (e.g. see Ayala et al. (2014), Parishani et al. (2015), and Wang and Maxey (1993)). It involves transformations of the velocity field between its representations

in physical space, $\mathbf{U}(\mathbf{x}, t)$, and spectral (Fourier) space, $\hat{\mathbf{U}}(\mathbf{k}, t)$, in order to perform some operations in the space that is most favourable. Detailed description of that method may be found in Appendix A. Note, that performing Fourier transforms (implemented as FFT) is the most computationally demanding part of the method. In the version of pseudo-spectral method used here, every iteration requires three 3D FFTs (1 forward and 2 inverse) for each component of the considered vector quantity and they dominate theoretical time complexity of the method, which is of order $N^3 \log N^3$ (per time step).

In the context of this study, pseudo-spectral method proves to be particularly effective method. Due to its use of spectral space and Fourier transforms it allows to easily incorporate large-scale forcing required to maintain homogeneous isotropic turbulence. For the same reason, it is also well-suited to be used with LES method, especially in a form that is proposed in this study (see Section 1.2), since velocity field filtering is defined in terms of convolution operation that becomes trivial to apply in Fourier space. Moreover, Fourier transforms that are repeatedly applied to fluid velocity field are consistent with periodic boundary conditions. Also, even though the velocity field is mainly integrated in the spectral space, it is also transferred back to the physical space (as opposed to purely spectral methods) and can be further used to calculate interactions between fluid flow and particles localised by their physical coordinates. Finally, pseudo-spectral method is known for its stability (if Courant-Friedrichs-Lewy number does not exceed 0.3) and superior computational accuracy for homogeneous isotropic turbulence (Peng et al. 2009). On the other hand, frequent use of Fourier transforms makes it difficult to be effectively implemented for massively parallel execution, as such operations require global access to data across computational subdomains. Such overheads for data transfer between processes rapidly increase with grid size, therefore it is important to find methods of reducing grid sizes as pseudo-spectral method does not seem to scale well performance-wise beyond grids of size $N = 1024$.

The context of simulations studied here requires steady homogeneous isotropic turbulence to be maintained throughout the entire computation. For that reason energy must be provided to the system in an adequate manner to make up for the losses due to dissipation inherent in turbulent processes and sustain statistically stationary flow that exhibits desired characteristics. Two main forcing schemes employed for that purpose are referred to as deterministic (Sullivan et al. 1994) and stochastic (Eswaran and Pope 1988). The effects of using both schemes on particle statistics (in OWC context only) were studied in Parishani et al. (2015) and Rosa et al. (2011, 2013, 2015). Slightly increased particle clustering and collision kernel values were observed with deterministic scheme, yet these discrepancies were deemed to be negligible, at least for the water droplets with radius smaller than 30 μm. Also, most discrepancies attributed to the choice of forcing scheme manifest when simulation time scale is correlated with forcing, which is partly alleviated by using time step, Δt, that is relatively small with respect to Kolmogorov time scale of turbulence, τ_k, as prescribed in Rosa et al. (2015) (here, $\Delta t/\tau_k \sim 10^{-2}$). Deterministic scheme, however, if properly parameterised, allows to achieve higher Reynolds numbers, R_λ, than by using stochastic forcing and this difference is important in this study. Hence, simulations performed here use only deterministic forcing scheme.

The basic idea behind deterministic forcing scheme, as laid out in Sullivan et al. (1994), is to set energy associated with largest eddies—or, equivalently, with lowest wavenumbers in the spectral space—to predetermined values in every time step. In order not to affect the entire flow this is done only for very few wavenumbers ($|k| \in \{1, 2\}$ in this study). Then, due to energy cascade that characterises inertial scales of turbulence, the energy injected at low wavenumbers is transferred to the higher ones allowing to achieve statistically stationary
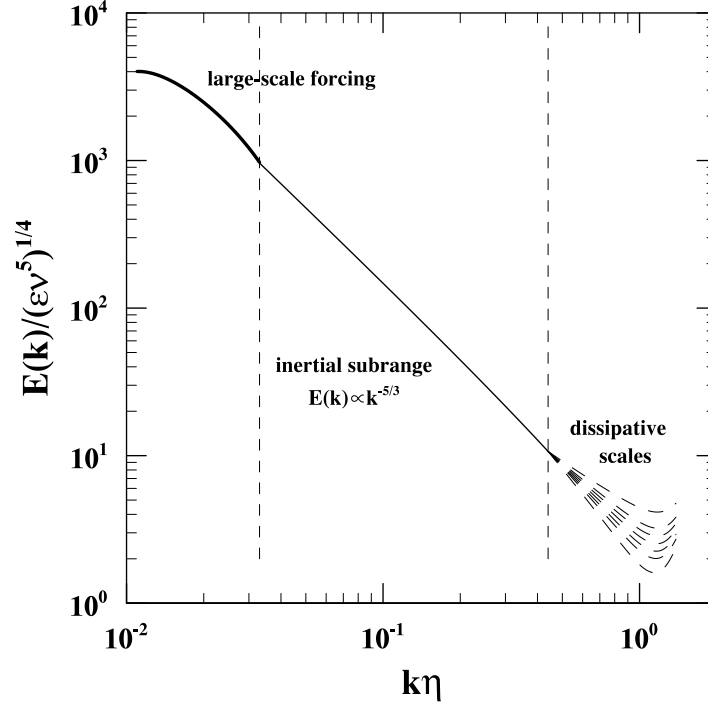
Figure 1.1: The basic idea of deterministic forcing scheme: energy is supplied on large scales by fixing it for small wavenumbers (bold line), then it is transferred following Kolmogorov energy cascade ($E(k) \propto k^{-5/3}$) in inertial subrange, to finally reach smallest dissipative eddies represented by largest resolved wavenumbers (when $k_{\mathrm{max}}\eta \sim 1 = 10^0$, diverging dashed lines) that have largest influence on measured particle statistics at contact distances. Both axes are using standard normalisations (see Section 2.1.2) and logarithmic scale, that makes $k^{-5/3}$ curves appear as straight lines.

state with desired characteristics of homogeneous isotropic turbulence (see Figure 1.1). It is accomplished by balancing large-scale energy input provided by the forcing term and energy depletion due to viscous dissipation at small scales. In case of this study, the contribution from the deterministic forcing, $\hat{\mathbf{f}}$, is included in Navier-Stokes equations in spectral space (see Equation **??** in Appendix A, that is a Fourier-transformed version of Equations 1.1). Here, following the setup used in Rosa et al. (2011, p. 6), the values for 3D shells associated with two lowest wavenumbers ($0.5 < |\mathbf{k}| < 1.5$ and $1.5 < |\mathbf{k}| < 2.5$) are set to 0.555440 and 0.159843 (following Kolmogorov's $E(k) \propto k^{-5/3}$ spectrum), respectively. For the remaining wavenumbers, $\hat{\mathbf{f}} = 0$, thus any smaller scales are not directly affected by forcing term.

1.2. Large-Eddy Simulations

The pseudo-spectral method, as described above, is used in DNS to directly calculate the velocity field of turbulent flow for all grid nodes. Despite important advantages, this method faces huge challenges in implementation for massively parallel execution (Onishi et al. 2013). Moreover, when applied to DNS it faces problematic limitations in computational performance and scalability. Therefore an alternative approach is proposed, so called large-eddy simulation (LES). The main goal is to reduce the size of computational grid without losing ability to model systems with similar range of turbulent scales, as measured by Taylor microscale Reynolds number, R_λ. This is achieved by directly resolving turbulent flow only for

large and intermediate scales and replacing direct resolution of small-scale turbulence (as it is done in DNS) with one of the proposed models of turbulence, referred to as subgrid-scale (SGS) model. Since we are replacing direct resolution with parameterisation, it is expected that the fidelity of results obtained using LES (when compared with DNS) may be diminished and they may be highly sensitive to the appropriate choice of the subgrid-scale model. On the other hand, this allows a significant reduction in the size of used grid and, consequently, either increase computational performance of current simulations or enable new ones that achieve much higher R_λ. This is possible because large part of computational effort in DNS is dedicated to resolving smallest turbulent scales (Pope 2000, p. 558). In case of this study, we use $N = 64$ for LES and $N = 256$ for DNS, thus the total number of grid nodes where fluid velocity field is directly resolved is reduced by the factor of 64 (while still achieving comparable values of R_λ). Conceptually, we may consider that each LES cell encompasses $4^3 = 64$ DNS cells where small-scale variations in velocity field would be directly resolved by integrating Navier-Stokes equations (see Figure 1.2).

DNS grid spacing (N=256)

LES grid spacing (N=64)

●——— **DNS** and **LES** nodes
○——— **DNS**-only nodes
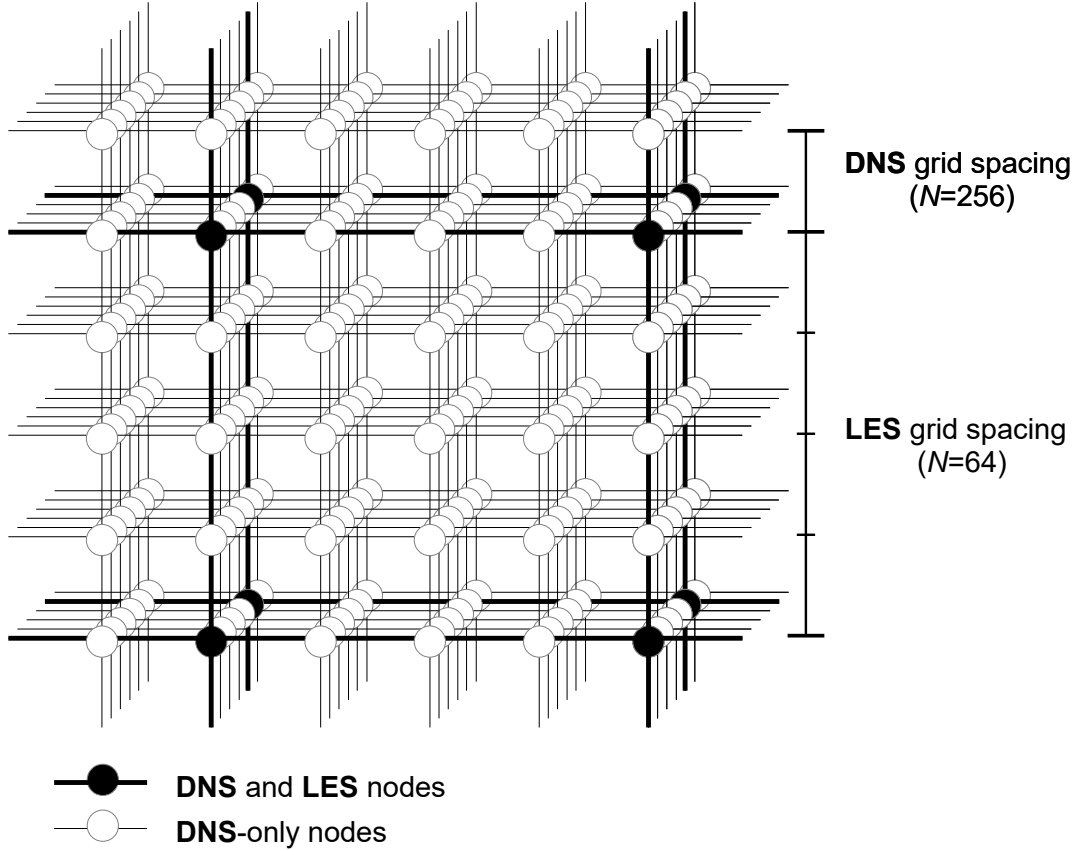
Figure 1.2: Conceptual juxtaposition of computational grids for DNS and LES. In LES, the subgrid-scale modelling parameterises small-scale turbulence that is directly resolved by $4 \times 4 \times 4$ block of cells in DNS.

In this study, that may be considered the continuation of Rosa and Pozorski (2017), a similar setup for LES method is employed (based on earlier work by Jin et al. 2010). In particular, the closure of the subgrid term is based on the concept of the spectral-eddy

viscosity, ν_e. In spectral space, thefiltered velocity field $\hat{\bar{\mathbf{U}}}(\mathbf{k}, t)$ is governed by the following momentum equation (Pope 2000)

$$\left\{ \frac{\partial}{\partial t} + [\nu + \nu_e(k|k_c)]k^2 \right\} \hat{\bar{\mathbf{U}}}(\mathbf{k}, t) = \mathbf{P}(\mathbf{k})\mathcal{F}(\bar{\mathbf{U}} \times \bar{\boldsymbol{\omega}}) + \hat{\mathbf{f}}(\mathbf{k}, t), \qquad (1.2)$$

where $\mathbf{P} \equiv \{\mathbf{P}_{ij}\}$ is the projection tensor (see Equation **??**) and $\mathcal{F}$ – Fourier transform. By k_c we denote cutoff wavenumber for filtering and its value is set using the same formula as maximal resolved wavenumber, $k_{\max}$, in DNS, i.e. $k_c = \lfloor (N-3)/2 \rfloor$ (for $N = 64$, we have $k_c = 30$). In this method of modelling turbulence a sharp spectral filter is used to separate filtered (resolved) and residual (modelled) velocity fields which are strictly separated from each other in the spectral space with $|\mathbf{k}| = k_c$ as the boundary. Hence, modelled modes for $|\mathbf{k}| > k_c$ have no bearing on turbulence model for larger wavenumbers and all necessary information on filtered velocity field $\hat{\bar{\mathbf{U}}}(\mathbf{k}, t)$ is contained in wavenumbers smaller than k_c. Conversely, filtered velocity field contains no information on residual (small-scale) motions, thus they have to be entirely modelled (Pope 2000, p. 615).

In Equation 1.2, the term $\nu_e(k|k_c)k^2\hat{\bar{\mathbf{U}}}(\mathbf{k}, t)$ represents the specific subgrid-scale model that is used for parameterisation of small-scale turbulence. Here, following Rosa and Pozorski (2017), a standard formula for the spectral eddy viscosity is used (see Chollet and Lesieur 1981). In particular, the eddy viscosity is given by

$$\nu_e(k|k_c) = \nu_e^+(k|k_c)\sqrt{\frac{E(k_c)}{k_c}}, \qquad (1.3)$$

where total spectral energy for threshold wavenumber, $E(k_c)$, is dynamically evaluated at each time step, while the remaining term depends on k and is defined as follows

$$\nu_e^+(k|k_c) = C_K^{-3/2}[0.441 + 15.2\exp(-3.03k_c/k)], \qquad (1.4)$$

where C_K is the model constant (here, we set $C_K = 2.5$).

LES is a well-established method in simulation of turbulent flows in many fields of research, and recently it is gaining more and more recognition as a tool for resolving carrier fluid flow in particle-laden simulations. The main issue with LES, i.e. the unavailability of turbulent velocity field for small dissipative scales, is not a huge concern for some experiments, mainly whene single-particle statistics are concerned, such as one-particle dispersion coefficient (Yang et al. 2008). Still, some single-particle statistics, such as average settling velocity, are affected by phenomena like preferential sweeping that depend on small-scale fluid motion, and thus are influenced by subgrid-scale modelling (Rosa and Pozorski 2017; Tom and Bragg 2019). Moreover, two-particle collision statistics are clearly influenced by small-scale velocity field that is missing in LES (Jin et al. 2010). In most cases, studies show that elimination of directly resolved fine-scale turbulence may influence preferential concentration of inertial particles (in cases covered by this thesis it is usually reduced, but it may also be amplified, see Fede and Simonin (2006) for more details). Several studies established that such dependence on small turbulent scales is most prominent when Stokes number, St, of the system is close to 1 (Jin et al. 2010; Pozorski and Apte 2009; Wang et al. 2000) and that is where most significant discrepancies between DNS and LES should manifest. In contrast to the particle concentration (as measured by the radial distribution function), other collision statistics, such as the radial relative velocity (see Section 2.2.1), are to some extent governed by particle interactions with large-scale eddies (Wang et al. 2000) and their accuracy

should be much less affected in LES. Determining the impact of LES parameterisation on such statistics is one of the main goals of this thesis. This overview, however, shows that establishing relations between particle statistics, the ranges of turbulent scales that affect them, and possible impact of filtering out contribution of small eddies on particle behaviour is a complex task.

Note, that Jin et al. (2010) and Rosa and Pozorski (2017) also consider intermediate method between DNS and LES that is referred to as either filtered DNS or LES *a priori*. It uses the same size grid as DNS and directly resolves turbulent flow for all scales, including the smallest. Such velocity field, however, before it is used to calculate momentum transfer to particles (see Equation 1.5) is filtered in spectral space by setting all values of $\hat{\mathbf{U}}(\mathbf{k}, t)$ to zero for large wavenumbers above filtering threshold (i.e. for $|\mathbf{k}| > k_c$). Hence, particles are affected by filtered flow without directly resolved small-scale turbulence, as in LES. On the other hand, the flow itself is evolved with the same resolution as in DNS, thus providing more precise evolution of the fluid velocity field. For the purpose of this study filtered DNS is not of great interest, since it requires grids as large as for DNS, hence it provides no viable improvement in method scalability and performance.

1.3. Modelling Interactions between Fluid Flow and Particles

The population of particles contained within given system is modelled using Lagrangian approach, so that each (computational) particle is individually tracked. Hence, given total number of particles, N_{part}, k-th particle, where $k \in \{1, \ldots, N_{\text{part}}\}$ is characterised by its position – $\mathbf{Y}^{(k)}(t)$, velocity – $\mathbf{V}^{(k)}(t)$, and other relevant properties, such as physical radius – $a^{(k)}$. In case of this study, not only radius of any single particle is constant throughout the entire simulation, but only *monodisperse* systems are considered, i.e. systems where all particles have the same size (that is $a^{(k)} = a$ for all k). Note that since Lagrangian tracking is employed, particles may assume any positions within domain, not only at locations of grid points where values of fluid velocity field are directly available. For that reason, proper interpolation techniques must be used when interactions between two phases are taken into account.

First, we consider advancement in time of velocity and position vectors of k-th particle affected by the carrier fluid with velocity field, $\mathbf{U}(\mathbf{x}, t)$. For systems with large enough ratio between particle and fluid density, such as atmospheric clouds, we may apply simplified equations of motion (Maxey and Riley 1983). For k-th particle we have

$$\begin{cases} \frac{d\mathbf{V}^{(k)}(t)}{dt} = -f(Re_p)\frac{\mathbf{V}^{(k)}(t) - \mathbf{U}(\mathbf{Y}^{(k)}(t), t)}{\tau_p} + \mathbf{g}, \\ \frac{d\mathbf{Y}^{(k)}(t)}{dt} = \mathbf{V}^{(k)}(t), \end{cases} \qquad (1.5)$$

where f is the drag correction factor (in this study $f = 1$), $Re_p = (2a\rho V_{\text{rel}})/\mu$ – particle Reynolds number, V_{rel} – particle–fluid relative velocity, $\tau_p = (2\rho_p a^2)/(9\mu)$ – Stokes inertial response time of a particle, ρ_p – particle density, μ – dynamic viscosity of the fluid, and ρ – density of the fluid. These equations, as stated before, hold when $\rho_p \gg \rho$ (in case of water droplets in air, $\rho_p/\rho \approx 10^3$). The gravitational acceleration is given as $\mathbf{g}$, which may be either zero (for simulations without gravity), or set to $980.67 \, \text{cm/s}^2$ and pointing vertically downwards. Furthermore, expression $\mathbf{U}(\mathbf{Y}^{(k)}(t), t)$ denotes contribution from the velocity field of the carrier fluid in the current location of k-th particle and it is calculated using six-point Lagrangian interpolation in each spatial direction (Ayala et al. 2014). Effects due to the finite size of physical, spherical particles (as opposed to idealised point-particle

representation) may be neglected, since considered range of water droplets radii (20–60 μm) makes them significantly smaller than the Kolmogorov length scale of the turbulence, η. Equations 1.5 are integrated using fourth-order Adams-Moulton and fourth-order Adams-Bashforth methods, respectively.

The procedure described above incorporates calculation of the particle motion, as well as the influence of the carrier fluid on particles due to momentum transfer. When simulations are limited to above description of fluid-particle interactions they are said to involve one-way momentum coupling (OWC). These simulations require less computational resources and have been shown to effectively model dilute systems. In general, we use particle mass loading, Φ_m, as the global measure of relative amount of particles in the system. It is defined as the ratio of total mass of particles to total mass of carrier fluid contained in the system, i.e.:

$$\Phi_m = \Phi_V \frac{\rho_p}{\rho} = \frac{(4/3)\pi a^3 N_{\text{part}}}{L^3} \frac{\rho_p}{\rho}, \tag{1.6}$$

where L denotes the side-length of simulation domain. Here, Φ_V denotes the particle volume fraction, which may be used as an alternative measure of amount of particles in the system. When particle content becomes larger (approximately, for $\Phi_m > 0.1$) OWC approach becomes insufficient and other interactions should be considered as well. Promising strategy, not discussed further in this study, is to account for interactions between particles through disturbance field that models aerodynamic interactions between particles, as in Hybrid DNS method (see e.g. Ayala et al. 2014). Another remedy is to account for the transfer of momentum in the other way as well, i.e. from particles to the carrier fluid. Such approach not only allows to study influence of particles on the fluid flow characteristics and turbulence modulation, but also, indirectly, provides a limited way to include interactions between particles that are mediated by the fluid flow disturbed by the presence of nearby, slowly approaching particles. These simulations are said to be performed under two-way momentum coupling (TWC).

In TWC approach, we assume that cumulative force per unit mass exerted by particles on the fluid, denoted by $\mathbf{f}^{(p)}$ (see Equation 1.1), is non-zero. Such contribution may be expressed as follows (Bosse et al. 2006; Monchaux and Dejoan 2017; Rosa et al. 2022)

$$\mathbf{f}^{(p)}(\mathbf{x}, t) = -\frac{M}{\rho_p} \sum_{k=1}^{N_{\text{part}}} m_p^{(k)} \left(\frac{\mathbf{U}(\mathbf{Y}^{(k)}(t), t) - \mathbf{V}^{(k)}(t)}{\tau_p} \right) \delta \left(\mathbf{x} - \mathbf{Y}^{(k)}(t) \right), \tag{1.7}$$

where most of the notation follows that from Equation 1.5, except $m_p^{(k)}$ which denotes individual mass of k-th particle. Moreover, M is the weighting (super-particle) factor, discussed later in this section. This continuous description involves summation of contributions from all particles (terms that, according to Newton's third law, are equal in magnitude and opposite in direction to terms in Equation 1.5) and localised in given spatial point $\mathbf{x}$ with Dirac delta distribution. In practice, we need a convenient way to calculate $\mathbf{f}^{(p)}$ for positions $\mathbf{x}$ at grid points without need to iterate over all particles. Due to mismatch between actual particle positions and discrete locations of grid points we use mollified Dirac delta, so that strict particle locality is relaxed and their contributions may be projected onto adjacent grid nodes. Thus, Equation 1.7 becomes

$$\mathbf{f}^{(p)}(\mathbf{x}, t) = -\phi_m(\mathbf{x}, t) \left(\frac{\mathbf{U}(\mathbf{x}, t) - \mathbf{V}_E(\mathbf{x}, t)}{\tau_p} \right), \tag{1.8}$$

where ϕ_m is local mass loading. The term $\mathbf{V}_E(\mathbf{x}, t)$, is referred to as Eulerian particle velocity

at location $\mathbf{x}$, and may be computed as follows:

$$\mathbf{V}_E(\mathbf{x}, t) = \sum_{k=1}^{N_{\text{part}}} \mathbf{V}^{(k)}(t)\, \sigma(||\mathbf{x} - \mathbf{Y}^{(k)}(t)||), \qquad (1.9)$$

where σ is the interpolation kernel used to determine effect of given particle, based on its location, $\mathbf{Y}^{(k)}(t)$, onto grid node located at $\mathbf{x}$. There are several choices of such kernels and their practical implementations (Garg et al. 2007), but in this study the projection onto neighbouring nodes (PNN) is used exclusively. Instead of summing all particle forces around a node, particle force contribution is projected onto eight neighbouring nodes based on some weighing scheme. Such scheme, in general, is a standard bi- or tri-linear function that depends on separation distance between particle and grid node. Here, in particular, we use calculations based on cell volume partition (see Figure 1.3) introduced in Squires and Eaton (1990). This interpolation procedure is justified when influence of particles on the fluid is indeed highly localised and limited to the closest neighbouring nodes. In practice, this takes form of the requirement that size (radius, a) of a particle must be smaller than both spatial grid spacing, Δx and smallest resolved turbulent scales as measured by Kolmogorov length scale, η. Both conditions are satisfied for all simulations in this study (see Section 2.1.3).

Note, as well, that in systems under TWC a mean flow must appear due to the net influence of all particles on the fluid (especially if gravity is concerned) That violates periodicity condition and leads to instability of computations. For that reason, at every time step, the Fourier mode corresponding to mean flow (i.e. for $|\mathbf{k}| = 0$) is set to zero, which is equivalent to applying a pressure gradient countering the mean flow and not affecting the validity of statistical results. Another numerical artefact of TWC is the indirect effect of $\mathbf{f}^{(p)}$ on the continuity equation that may cause resulting velocity field to be not divergence-free. This issue was addressed in Rosa et al. (2020) and it turns out that this effect is not significant in simulations performed here, since the volume fraction of particles compared to the fluid is relatively small (at most of order 10^{-3}). Moreover, computations involved in the pseudo-spectral method enforce constraint from continuity equation by projecting the velocity vector onto plane normal to 3D wavenumber $\mathbf{k}$ (which also eliminates direct dependence on pressure, see Appendix A for more details).

The total number of particles, N_{part}, is another parameter, besides grid size N, that mainly determines computational burden of simulations. In this study, highest number of individually tracked particles was 20 million and for droplets with smaller radii that was still not sufficient to achieve higher values of the mass loading. Still, simulations with larger mass loading ($0.1 < \Phi_m < 1$) are necessary to clearly observe effects of two-way momentum coupling on measured statistics. For that reason, in some simulations, super-particle parameterisation was used to increase Φ_m without adding new computational particles (Elghobashi 1994). That parameterisation is applied by using weighting factor, M, in Equation 1.7. When $M = 1$ each computational particle represents exactly one dropletand no extra parameterisation is involved. For $M > 1$, however, every computational particle models a cluster of M droplets (i.e. the super-particle) that is tracked together as a single point-particle with inflated mass by the factor of M.

Such parameterisation was used in Rosa et al. (2020) for similar reasons and it was observed that it does not significantly affect measured collision statistics as long as M is not too large. Moreover, it was noted that these discrepancies are relatively small when mass loading is large, this is probably due to the stronger turbulence attenuation in simulations without gravity (turbulence is the main mechanism enforcing particle clustering). On the other hand, in simulations with gravity a larger mass loading results in the formation of new vortical
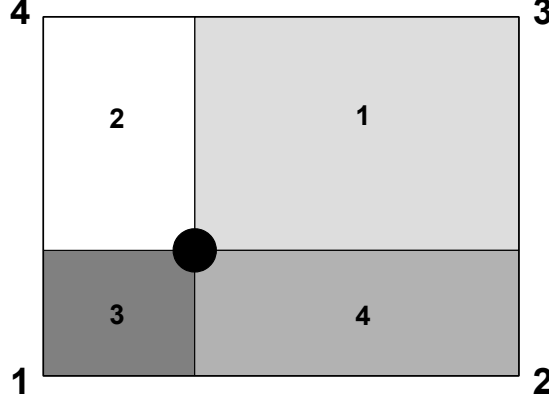
Figure 1.3: Projection onto neighbouring nodes (PNN; simplified illustration for 2D case). The contribution of the particle momentum to the fluid momentum at a grid node depends on the separation distance. For example, the particle force may be projected onto neighbouring nodes using weights that are proportional to cell areas (or volumes in 3D case). Here, the fluid flow at grid node 1 is affected by a fraction of the particle Stokes drag proportional to the area with marker 1, and so on. Based on Garg et al. (2007, Fig. 1 therein).

structures which cause the decorrelation of particle motion and consequently a more uniform spatial distribution. More systematic analysis of the impact of this parameterisation was conducted in a recent study by Rosa et al. (2022) where collision statistics from simulations with varying M and fixed mass loading, Φ_m, were analysed. The clear tendency for that parameterisation to overestimate the radial relative velocity and underestimate the radial distribution function was reported. For values of $M < 20$ the influence of super-particle parameterisation may be acceptable, but otherwise discrepancies rapidly cumulate and render obtained results applicable for only qualitative analysis at best (in some cases, for $M = 100$, values of RDF were halved, and for RRV inflated by the factor of 3). Moreover, even larger discrepancies were observed in simulations with gravity.

Interestingly, some studies using more refined techniques of dealing with super-particles (Garg et al. 2009) have shown that errors arising from that parameterisation increase with refinement of the grid. This may be beneficial when considering LES method, as it works on much coarser grid than comparable DNS. Still, cumulative effects and possible interactions between these two parameterisations may be quite complex and hard to follow in a systematic and quantitative manner.

1.4. Notes on Implementation

The effective implementation of methods presented above is necessarily intended for massively parallel computation environments (supercomputers) due to large grids and particle populations that are required to produce physically meaningful results. The solver code used in this study was long developed, tested, and improved upon to provide further capabilities (see e.g. Ayala et al. 2014; Parishani et al. 2015), including modifications necessary to obtain results presented here. It is implemented using Message Passing Interface (MPI) to facilitate communication between several processes executing the code. The division of work is based on the concept of 2D domain decomposition where each process is handling all computations associated with one part (subdomain) of the entire computational domain. In this case, the

domain is divided along two out of three spatial axes into "columns" with equal number of grid nodes (see Figure 1.4). By default, two directions chosen for such decomposition are those orthogonal to the (vertical) direction of gravity, in order to minimise the number of particles crossing subdomain boundaries. This strategy is relatively simple to implement and quite efficient, at least if we assume that distribution of particles between subdomains is close to uniform (this assumption will be further analysed in Section **??**). In this study, subdomains have dimensions $16 \times 16 \times N$ to provide large enough margin for convenient communication between processes. In particular, for DNS and its grid with 256^3 nodes we have $16^2 = 256$ subdomains, and for LES with 64^3 grid nodes – $4^2 = 16$ subdomains. The number of processes used to execute solver code is equal to the number of subdomains used.
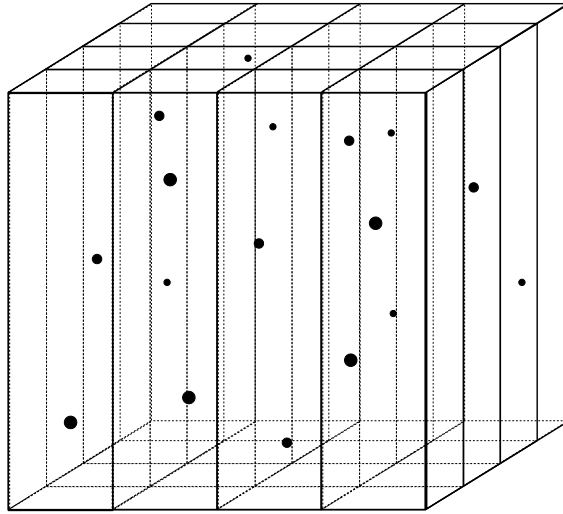

Figure 1.4: Schematic representation of 2D domain decomposition. This image corresponds to the actual decomposition of 64^3 grid used for LES. Entire domain is divided into $4 \times 4 = 16$ subdomains, each with $16 \times 16 \times 64$ nodes.

Exact steps that constitute each iteration of both DNS and LES method are summarised in Table **??**. In general, entire code may be divided into parts that handle computations involving either fluid flow or particle motion, as well as parts used for data postprocessing (i.e. to calculate and output interesting statistics of fluid flow and particles). The heart of pseudo-spectral code is the efficient implementation of the fast Fourier transform, as every iteration requires performing 3D FFT three times. Parallel implementation of 3D FFT is used as proposed by Ayala and Wang (2013). It is decomposed into three separate calls to 1D FFT procedures provided by `fftw` library together with an original procedure for data transposition. The choice of 2D domain decomposition was mainly driven by the fact that it was found to be optimal for such implementation of parallel 3D FFT. It was chosen above 1D decomposition that was initially proposed by Dmitruk et al. (2001), since it heavily restricted number of parallel processes allowed to execute the code, and above 3D decomposition which introduced excessive costs of communication and data transfer between larger number of subdomains (Ayala and Wang 2013). The architecture used to store particle data and transfer it between processes is a key part of the implementation, as detection of nearby particles is crucial for efficient calculation of two-point particle collision statistics. For that reason the concept of linked lists together with the cell-index method was employed according to Allen and Tildesley (1987, p. 149–152). In every run statistics of the fluid flow and particles

statistics are gathered only after the entire system has reached the statistically stationary state, which is not earlier than after approximately $10T_e$ (Rosa and Pozorski 2017), where T_e is turnover time for largest resolved eddies.

Chapter 2

Physical Fidelity of DNS and LES Results

This Chapter focuses on ascertaining the physical fidelity of LES results in comparison with those provided by DNS. Since LES partially replaces direct resolution of flow with subgrid-scale parameterisation, some difference of results is expected. This is also true for particle statistics at contact distance, as they are especially sensitive to the effects of turbulence at smaller length scales. In this chapter, basic statistics and energy spectra of background turbulent flow shall be presented for both methods, followed by particle statistics and the effects of turbulence modulation by particles in TWC simulations. More importantly, broader analysis of key particle collision statistics—radial distribution function, radial relative velocity, and collision kernels—is provided with results from both DNS and LES. Simulations with both one- and two-way momentum coupling are considered, both with and without gravity.

2.1. Turbulent Flow Statistics

The standard procedure in simulations using the pseudo-spectral code introduced in Chapter 1 is, at first, to obtain statistically stationary fluid flow without particles and estimate its statistics as a baseline. These statistics are discussed in two following sections. Later, such background flow is randomly seeded with particles and the entire system is simulated until stationary state is restored. At that point particle statistics may be collected. Such approach not only reduces time required by particle-laden simulations to achieve desired state but also provides a point of reference for studying influence of particles on the statistics of underlying turbulence in siumulations under two-way momentum coupling..

2.1.1. Basic Statistics of Turbulent Flow

When no specific boundaries are defined, the model of homogeneous and isotropic turbulence is abstracted from any physical scale. More precisely, without introduction of any reference objects with well defined physical dimensions (e.g. domain boundaries, or – as in this study – particles with well defined physical radii) turbulence parameters may be applied at arbitrary scales, from small cells of clouds to the global atmospheric circulation. For that reason, parameters and statistics of turbulent flow presented below are expressed in nondimensional spectral (DNS) units, as the most important indicator is the range of turbulent scales being resolved and not physical size of the domain. It should be added that the characteristic length scale results from the domain size. In turn, the time and velocity scales are determined by

the rate at which kinetic energy is supplied by the forcing scheme.

There are three main numeric parameters that influence the resulting turbulent flow and its statistics that are, for the most part, fixed for all simulations in this study. These include:

- the number of spatial grid nodes in each dimension, N, which primarily determines range of turbulent scales that can be directly resolved in simulations (here $N = 256$ for DNS and $N = 64$ for LES);

- the numerical (molecular) kinematic viscosity of the fluid, ν, is an important parameter that is required to balance out the large-scale forcing with enough energy dissipation to obtain viable energy spectrum and desired range of resolved scales of turbulence; in all simulations value of 1.5×10^{-3} is used, as it ensures numerical stability and maximises obtained Reynolds number;

- the time step, Δt, ensures numerical stability of the simulation.

Note that for the particle-free flow time step must be set to a value that guarantees that Courant number is lower than 0.3, which is established as a stability and accuracy threshold for the pseudo-spectral method. Recall, that Courant (or Courant–Friedrichs–Lewy, CFL) number is defined as follows:

$$\text{CFL} = \max(||\mathbf{U}||_1)\frac{\Delta t}{\Delta x},$$

where $|| \cdot ||_1$ is a 1-norm, maximum of which is taken over all nodes in the grid, and Δx is spatial spacing, here equal to $(2\pi)/N$. The default time step for most simulations was set to 9×10^4, but in some cases, due to complex interactions with particles, certain adjustments were necessary (for more details, see discussion in Section 2.1.3).

Beyond purely quantitative parameters there are some more "structural" choices that implicitly affect simulations and their results. One such important choice involves type of forcing scheme being used (here we exclusively use deterministic scheme, see Section 1.1). Even more options come with LES method, since the choice of subgrid-scale model being used is crucial for the final outcome of simulations. As discussed in Section 1.2, this study employs spectral-eddy viscosity model that was already used in several previous studies (Jin et al. 2010; Rosa and Pozorski 2017; Yang et al. 2008). Such model allows for some degree of customisation via model parameter C_K (see Equation 1.4) which in this study is fixed at 2.5. Note, that all aforementioned studies used only stochastic forcing and this one, according to author's knowledge, is the first where LES is used with deterministic forcing scheme (with pseudo-spectral solver). For that reason, extra effort was made to validate proper choice of C_K parameter as elaborated in Appendix B.

To gain some insight into properties of turbulence, we gather some standard flow statistics that are time-averaged over some period in which statistically stationary state of the flow was attained, and volume-averaged over the entire domain. Firstly, two basic statistics that are calculated directly from velocity field and energy spectrum of the flow are:

- u' – root-mean-square (RMS) fluctuating velocity – standard deviation of the fluid velocity field with respect to the mean flow (which is ensured to be zero); physically, it is related to the intensity of turbulence; and

- ϵ – energy dissipation rate – rate at which turbulence kinetic energy is converted into thermal internal energy; it may be computed as follows:

$$\epsilon = 2 \int_{k_0}^{k_{\max}} \nu k^2 E(k) dk \tag{2.1}$$

where $E(k)$ denotes the turbulent kinetic energy associated with wavenumber k in the spectral space, and ν is numerical kinematic viscosity.

Furthermore, some derived statistics that are commonly used to characterise different scales of turbulence are provided. These include: η – the Kolmogorov length scale, τ_k – the Kolmogorov time scale, L_s – the integral length scale, λ – the transverse Taylor microscale, T_e – the large-eddy turnover time. Finally, two important control and target statistics (besides CFL) are computed. These include:

- $R_\lambda = u'\lambda/\nu$ – Taylor-microscale Reynolds number – Reynolds number associated with inertial subrange and used to measure the range of resolved turbulent scales (in this study, this value is meant to be maximised given fixed grid scale N); and

- $k_{\max}\eta$ – spatial resolution parameter that serves as an important control value in DNS; it should be minimised in order to maximise amount of resolved turbulence (i.e. R_λ), but its value must be greater than 1 to ensure that fine scales of turbulence can be resolved.

Note, that for studies oriented towards maximising R_λ (as this one is) it is customary to aim for $1 < k_{\max}\eta < 2$, but in other studies resolution requirements may differ (Buaria et al. 2019) as higher values of $k_{\max}\eta$ ensure that simulations are more numerically stable. Also, in TWC simulations it is argued that larger values of $k_{\max}\eta$ may be associated with more stability in inter-phase interpolation (see Rosa et al. 2020).

Table 2.1 contains defining parameters and gathered statistics of background turbulent flows for both DNS and LES. The measurement uncertainties for these statistics were calculated as in Rosa et al. (2013), accounting for the autocorrelation of flow statistics in the statistically stationary state. The parameters introduced above are calculated in a way specific for DNS simulations, hence may not directly translate to LES flows but still serve as helpful indicators when comparing two methods (especially, R_λ). There is no agreement between authors whether to present more (Rosa and Pozorski 2017) or less (Yang et al. 2008) of such DNS statistics for LES as well. This is mainly due to the dependence of many statistics on numerical viscosity, ν, which is modelled in subgrid-scale model and depends on the wavenumber, k (see Equation 1.3), not being constant as in DNS. For that reason, most of statistics for LES in Table 2.1 (marked with asterisk) are listed with "effective" values which are calculated in a way that accounts for subgrid-scale modelling on viscosity (see Appendix B for details).

First two columns refer to particle-free flows used for all simulations in this study, DNS and LES, respectively. The remaining column is provided as a reference and for validation of results. DNS turbulent flow was simulated with similar parameters to the one used for numerical experiments with one-way momentum coupling in Rosa et al. (2013, Table 1, entry for 256^3), which are presented in third column of Table 2.1. Note that slightly smaller value of viscosity used in that study resulted in smaller resolution parameter and, consequently, $\sim 15\%$ larger Reynolds number. Particularly interesting is the comparison between statistics for DNS and "effective" statistics for LES. For ones that are directly derived from either fluid velocity field, u', or its energy spectrum, ϵ, there is strong agreement. The same is true for large scale parameters, L_s and T_e. What is most important, despite much smaller grid size, the R_λ in both cases is almost the same due to the effects of spectral-eddy viscosity of subgrid-scale model. Also, u', that is directly computed from fluid velocity field (independet from ν) and associated with the magnitude of turbulence assumes very close values for both DNS and LES. On the other hand, we can see increase (approximately by the factor of 2) in

	DNS	**LES***	Rosa et al. (2013) **DNS**
N	256	64	256
$\Delta t \cdot 10^4$	9.0	9.0	9.0
$\nu \cdot 10^3$	1.5	1.5	1.1
u'	0.871 ± 0.001	0.861 ± 0.001	0.868 ± 0.002
ϵ	0.212 ± 0.002	$0.200 \pm 0.001*$	0.200 ± 0.003
$\eta \cdot 10^2$	1.125 ± 0.003	$2.078 \pm 0.007*$	0.903 ± 0.037
$\tau_k \cdot 10^2$	8.436 ± 0.043	$15.755 \pm 0.122*$	7.420 ± 0.620
L_s	1.462 ± 0.003	1.501 ± 0.004	1.496 ± 0.005
$\lambda \cdot 10$	2.851 ± 0.011	$5.252 \pm 0.014*$	2.494 ± 0.015
T_e	3.616 ± 0.028	$3.697 \pm 0.025*$	3.774 ± 0.045
$k_{\max}\eta$	1.423 ± 0.004	—	1.143 ± 0.005
R_λ	165.91 ± 0.51	$165.01 \pm 0.11*$	196.87 ± 0.78

Table 2.1: Parameters and statistics, in spectral units, of background turbulent flows simulated in this study (first two columns) and from Rosa et al. (2013) shown for results validation (third column). All listed simulations used deterministic forcing scheme.
* – in LES, statistics marked with * are "effective", i.e. calculated using viscosity adjusted by subgrid-scale model; for more details see Appendix B.

spatial and temporal scales (both small, η and τ_k) and intermediate (λ). No previous LES statistics are presented for comparison, as in e.g. Rosa and Pozorski (2017, Table 1 therein), since all of these studies employed stochastic forcing scheme which makes obtained statistics not directly comparable.

2.1.2. Energy and Dissipation Spectra

The important insight and validation for any simulation of turbulent flow is the analysis of its energy and dissipation spectra. Since the pseudo-spectral method naturally operates in Fourier space the energy spectrum, $E(k)$, can be easily retrieved. Such spectrum, for intermediate wavenumbers, may be compared with theoretical Kolmogorov spectrum. More specifically, for inertial subrange, we expect obtained spectra to closely coincide with:

$$E_{\text{Kolm}}(k) = C\epsilon^{2/3}k^{-5/3}, \tag{2.2}$$

where constant C was experimentally determined to be 1.5. Furthermore, the energy dissipation spectrum, $D(k)$, may be easily derived for $k \in \{k_0, \ldots, k_{\max}\}$ using the following formula:

$$D(k) = 2\nu k^2 E(k).$$

Energy and dissipation spectra of turbulent flows obtained by DNS and LES are shown in Figures 2.1 and 2.2, respectively. For convenience, both spectra are shown using log-log plot with proper normalisation to ensure that values are dimensionless.

Figure 2.1 clearly shows that both energy spectra follow theoretical Kolmogorov spectrum in the inertial subrange (reference line is shifted for clarity). For LES, however, slight underestimation of the energy for intermediate wavenumbers may be observed. This effect is expected (Jin et al. 2010) and it is attributed to the overdissipation of energy inherent in the spectral-eddy viscosity model. Such increase of dissipation rate for wavenumbers close to
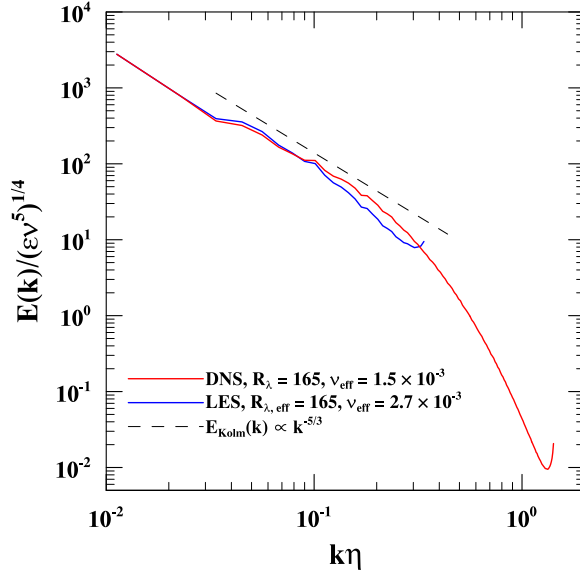
Figure 2.1: The normalised energy spectra of background turbulent flows for both DNS and LES. Dashed line provides comparison with $k^{-5/3}$ curve of theoretical Kolmogorov spectrum (see Equation 2.2) for inertial subrange.

filtering threshold, $k_c = 30$, may be better observed on Figure 2.2, where respective dissipation spectra are shown. It follows the region where $D(k)$ for LES is significantly smaller due to the smaller overall energy contained in these wavenumbers, as the energy is more strongly dissipated in larger modes (for $k\eta < 0.1$) due to contributions from the spectral-eddy viscosity. This also manifests in a shift of the maximum of $D(k)$ which occurs for smaller wavenumbers than for DNS where such peak is observed around $k\eta \approx 0.2$, which coincides with previous simulations and experimental results (Wang and Maxey 1993). Such discrepancies between DNS and LES in dissipation rates throughout inertial subrange may affect other properties of turbulent flow, as well as particle collision statistics. Another peculiar characteristic of energy spectra is the sudden increase of energy for largest wavenumbers (close to $k_{\max}$ for DNS, or k_c for LES). Rosa and Pozorski (2017) observed similar artifacts and suggested that they are due to accumulation of energy in the high-wavenumber modes, since the transport of energy is limited there by the viscous suppression.

2.1.3. Parameters of Particle-Laden Flows

When simulation of background turbulent flow reaches the statistically stationary state, as described in Section 2.1.1, individually tracked particles are introduced into the system with the uniform spatial distribution and inheriting velocity from the local fluid flow. In this study, the focus is on atmospheric clouds, where particles represent small water droplets (of radii ranging from 20 μm to 60 μm) and the carrier fluid is atmospheric air. Note, that for the remainder of the thesis terms "particles" and "droplets" shall be used interchangeably. These particles confine simulations to specific physical dimensions and such conversion of spectral DNS units to physical units is based on matching the Kolmogorov scales. In this study, we set: $\nu_{\text{air}} = 0.17\,\text{cm}^2/\text{s}$ and $\epsilon_{\text{cloud}} = 400\,\text{cm}^2/\text{s}^3$, which correspond to conditions observed in clouds with moderate to strong convection. In these conditions the side length of domain under consideration turns out to be approximately 33 cm.

For particle-laden flows, in general, the statistics of droplets are mainly functions of three
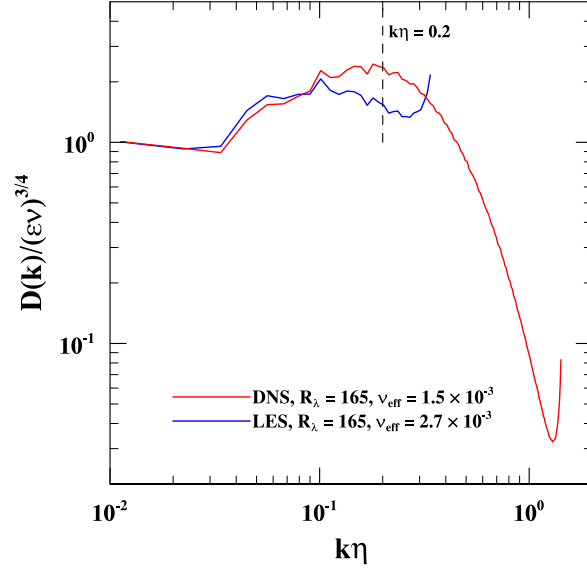
Figure 2.2: The normalised energy dissipation spectra of background turbulent flows for both DNS and LES. Point where $D(k)$ is expected to be maximal (for $k\eta = 0.2$) is marked by dashed line.

independent nondimensional parameters. Firstly, the particle inertia can be expressed in terms of the Stokes number, $St = \tau_p/\tau_k$, defined as the ratio of the inertial response time to the Kolmogorov time scale. Furthermore, the range of scales of turbulence in the system which affects particle behaviour is measured by Taylor-microscale Reynolds number, R_λ, as defined in Section 2.1.1, which is similar for all simulations under OWC (both DNS and LES) at approximately 165. Finally, when settling particles are considered, we use normalised terminal velocity, $S_V = V_T/v_k$, that is the particle still-fluid terminal velocity, V_T, normalised by the Kolmogorov velocity scale, $v_k = \eta/\tau_k$. Note, that independence of these parameters remains true for simulations under one-way momentum coupling. This picture, however, becomes more complex when two-way coupling is considered. When effects of particles on the flow are taken into account, these parameters become indirectly dependent, e.g. large settling particles (with larger St and S_V) are known to create additional vortical structures in flow, affecting R_λ, which—in turn—may alter settling velocity of particles (and, thus, S_V).

a [μm]	20	25	30	35	40	45	50	55	60
St	0.254	0.396	0.571	0.777	1.015	1.284	1.585	1.918	2.283
S_V	1.789	2.790	4.018	5.468	7.143	9.040	11.160	13.504	16.071
Fr	0.81	3.08	9.21	23.23	51.76	104.93	197.44	349.77	589.54
η/a	29.60	23.69	19.73	16.91	14.80	13.16	11.84	10.76	9.87
$\Delta x_{\text{DNS}}/a$	64.58	51.67	43.06	36.90	32.29	28.70	25.83	23.48	21.53
$\Delta x_{\text{LES}}/a$	219.62	175.70	146.42	125.50	109.81	97.61	87.85	79.86	73.21
$\Delta t/\tau_p \times 10^2$	17.21	11.02	7.65	5.62	4.30	3.40	2.75	2.28	1.91

Table 2.2: Basic parameters for particle-laden flows for the range of particle radii (in μm) that were used in this study. S_V and Fr are only applicable to simulations with gravity. Note, that values of $\Delta x/a$ ratio are listed separately for DNS and LES, since their spatial step Δx differ significantly due to much smaller density of grid points in LES without changing domain size.

Theses parameters are presented in Table 2.2 for simulations in this study, relative to droplet radii. In addition, the Froude number, Fr, is defined as the ratio of particle response

time to the residence time of the particles in a Kolmogorov eddy. Its value, however, may be expressed in terms of basic parameters introduced above, as $Fr = St \cdot S_V^2$. Properties of general particle-laden flows are often dependent on density ratio of two phases, but due to focus of this study on atmospheric phenomena, such ratio remains constant, as

$$\frac{\rho_p}{\rho} = \frac{\rho_{\text{water}}}{\rho_{\text{air}}} = \frac{1 \, \text{g/cm}^3}{0.001 \, \text{g/cm}^3} = 10^3.$$

For a broader picture, an extended analysis concerning the influence of particle–fluid density ratio on the dynamics of finite-size particles in homogeneous isotropic turbulent flows can be found in **Shen2021empty citation**. Since the density ratio is fixed in this study the particle mass loading, Φ_m, is exclusively used as a measure of relative amount of particles in a system as it is directly related to the volume fraction by $\Phi_V = \Phi_m \cdot 10^{-3}$ (see Section 2.1.3). On that note, whenever necessary to obtain systems with larger mass loading, the super-particle parameterisation (where single computational particle represents several physical particles) was used. For more information in which simulations super-particles were applied, see Appendix C.

Table 2.2 also includes some spatial and temporal ratios used as control parameters. Relatively large values of η/a and $\Delta x/a$ indicate that indeed particles used in these simulations are very small when compared to both computational grid cells and smallest scales of turbulent eddies. This second observation is paramount, as it not only makes the point-particle approximation justified. It is also important for simulations under two-way momentum coupling, as it allows all computations of the interphase momentum transfer to use a simplified model that is valid under assumption that indeed $a \ll \eta$, making additional corrections not necessary (**Horwitz2016**).

Due to the influence of momentum transfer from particles to the fluid some simulations under two-way momentum coupling required reduction of time step to preserve numerical stability of the simulation. The base value used ($\Delta t = 9 \times 10^{-4}$) takes into account the presence of particles (**Zhou2001**) and is adjusted for interactions between particles (as modelled by their hydrodynamic interactions) by satisfying condition $\Delta t/\tau_p < 0.15$, where τ_p denotes particle response time, that was suggested by Ayala et al. (2007). Only slight exceptions are simulations with the smallest droplets (20 μm) where this ratio is 0.17. Despite that, for some simulations Δt needed to be further reduced even by a factor of 4. This was most common for simulations with settling particles and high super-particle factor, M, that often coincided with high particle mass loading. These problems with stability appear to be caused by spikes in values of velocity field gradient that are inflated by momentum transfer from particles (i.e. $\mathbf{f}^{(p)}$ term in Equation 1.1) It locally saturates capabilities of the pseudo-spectral method and destabilises entire simulation (or, in other words, pushes "effective" CFL beyond required threshold of 0.3).

These issues require separate, more systematic treatment, but based on the experimental data obtained in this study (i.e. observation of cases where Δt required adjustment) some initial observations may be put forward. First of all, the risk of such oversaturation is related to the average number of particles per grid node which depends on the total number of particles and their masses (radii), as well as simulation method that was used. As outlined before, we employ LES to model turbulence with similar characteristics as by DNS with higher grid resolution. Still, the domain for both methods is being populated with the same number of particles. Hence, with grid sizes used here, it means that on average 64 times more particles influence single node in LES than in DNS. Moreover, this is exacerbated by preferential particle concentration (as measured by radial distribution function, see Section 2.2.1) that makes some nodes more saturated by particles than others.

In similar fashion, the super-particle parameterisation (i.e. when $M > 1$) may introduce non-physical clustering effect as single computational particle carries M times more momentum. This effect may be even more pronounced, since projection of particle momentum onto nearest neighbouring node depends on its distance to the position of that node. For large values of M much larger mass is concentrated at a single point which may happen to be located very close to an actual node and impart its huge momentum contribution, causing affected node to be oversaturated. For smaller M (ideally $M = 1$) particle mass is expected to be more evenly distributed around node locations, thus making such adverse occurrences statistically much less likely.

Finally, when the motion of particles is statistically anisotropic and their velocity is on average larger in one particular direction, their contributions to the fluid motion are less likely to cancel each other and are amplified in that direction. This is exactly the case of settling particles where gravity introduces such anisotropy. This explains why instabilities discussed here (and necessary reductions in Δt) were observed much more frequently for simulations with gravity.

All above observations are purely qualitative and deeper analysis of these issues was beyond the scope of this study. Even though further study is encouraged, due to complex nature of interactions between two phases in TWC simulations it is difficult to predict whether simple criterion depending solely on τ_p can be established here, especially when additional parameterisations (LES, super-particles) are considered.

2.1.4. Effects of Particles on Turbulence Modulation

When statistics of turbulent flow (see Section 2.1.1) are concerned, they remain unaffected by the presence of particles in the system unless two-way momentum coupling is included. In case of TWC simulations such effects are observed and are usually referred to as turbulence modulation due to particles. Such effects were systematically studied for DNS in Rosa et al. (2020). In this section a similar range of results is presented, expanding it by these obtained using LES. The comparison of LES and DNS results may be particularly illuminating since most of the momentum transfer from fluid to particles is usually attributed to the smallest scales of vortical structures and these depend on the quality of subgrid-scale model parameterisation in LES. This is especially true for smaller particles as their dynamics is mainly governed by fine turbulent structures. For more involved discussion on the physical interpretation of these results, see Rosa et al. (2020). Here, the focus is on the comparison of already established results from DNS with those obtained in this study using LES.

Figures 2.3 and 2.4 show effects of particles in TWC simulations on energy and dissipation spectra of the underlying turbulent flow. All simulations were performed with particles with radius of 40 μm and with varying mass loadings. Reference spectra from simulations without two-way momentum coupling were provided with dashed black lines. Results for DNS (top plots) show agreement with corresponding results in Rosa et al. (2020, Figures 4 and 5 therein). Moreover, in this study data from simulations with higher mass loading is presented (there, it was limited to $\Phi_m = 0.747$) and in all cases trends that were already observed continue further with the increase in Φ_m.

Results of LES show promising alignment with those from DNS. It is important to recall that energy and dissipation spectra are only available directly for a smaller range of wavenumbers in LES and it coincides with the part of DNS spectrum for approximately $k\eta < 0.25$. For non-settling particles this is the part of energy and dissipation spectra in DNS that decrease with increasing mass loading and it is also reflected in results for LES. Similarly, when effects of gravity are included, a sharp increase in both spectra throughout all modes (for $|\mathbf{k}| > 2$)
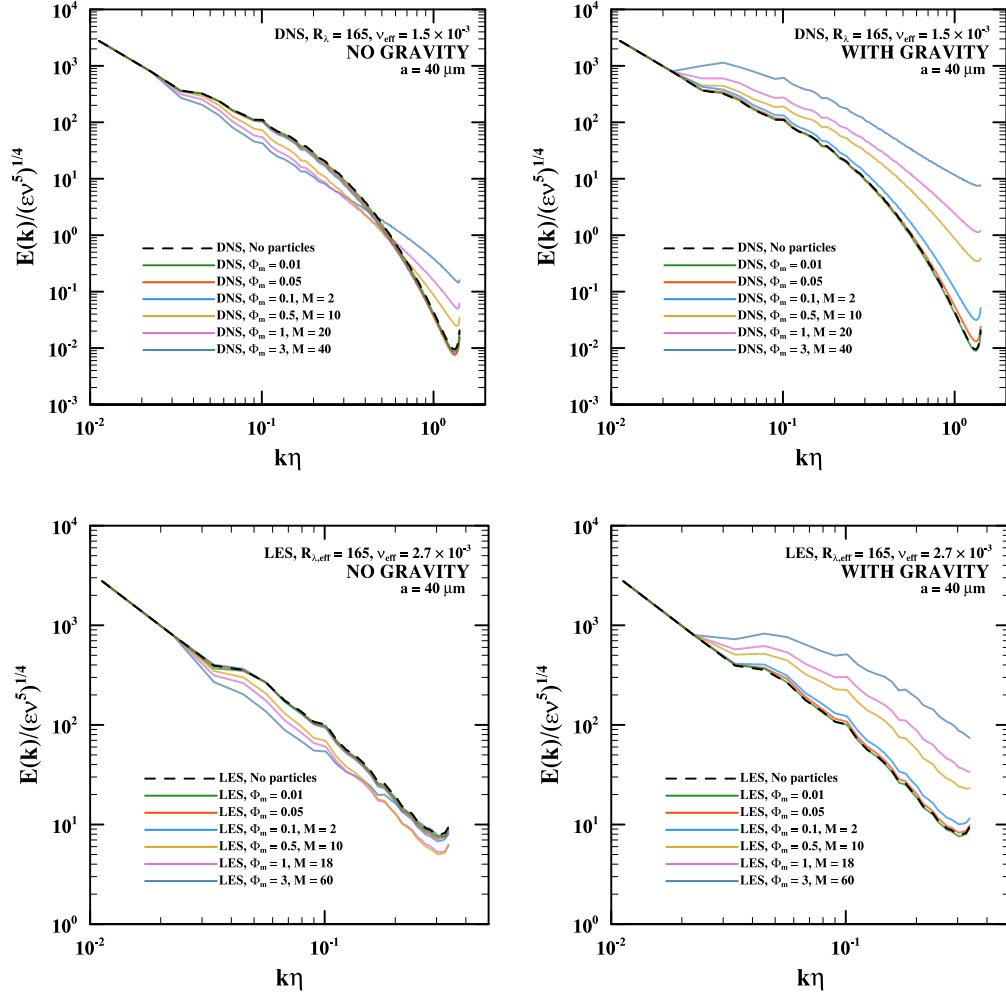
Figure 2.3: The normalised energy spectra of turbulent flows with droplets of radii 40 μm, with and without gravity, as obtained using both DNS and LES with two-way momentum coupling and different particle mass loadings. Dashed lines represent spectra without turbulence modulation by particles (see Figure 2.1). For comparison (with DNS results only), see Rosa et al. (2020, Figure 4 therein).

is witnessed, as expected.

The dual influence of TWC on energy spectrum for non-settling particles is known as "pivoting" (Bosse et al. 2006; Rosa et al. 2020; Squires and Eaton 1990). The kinetic energy of fluid is suppressed for intermediate wavenumbers due to increased energy dissipation while it is increased for high wavenumbers due to combined effects of larger viscous dissipation and transfer of momentum from the particles to the fluid. The increase of energy for small turbulent scales cannot be adequately represented in LES, in part due to the fact that the subgrid-scale model is agnostic to any momentum transfer from particles. Similar remarks are valid for settling particles but here the increase due to transfer of momentum from particles is larger and present throughout wide range of wavenumbers and such transfer affects even intermediate turbulent scales that are directly resolved in LES.

In addition to aforementioned spectra, Figure 2.5 shows impact of turbulence modulation on two specific statistics—RMS fluctuating velocity and energy dissipation. Results are normalised using respective statistic for simulations without two-way coupling,and plotted
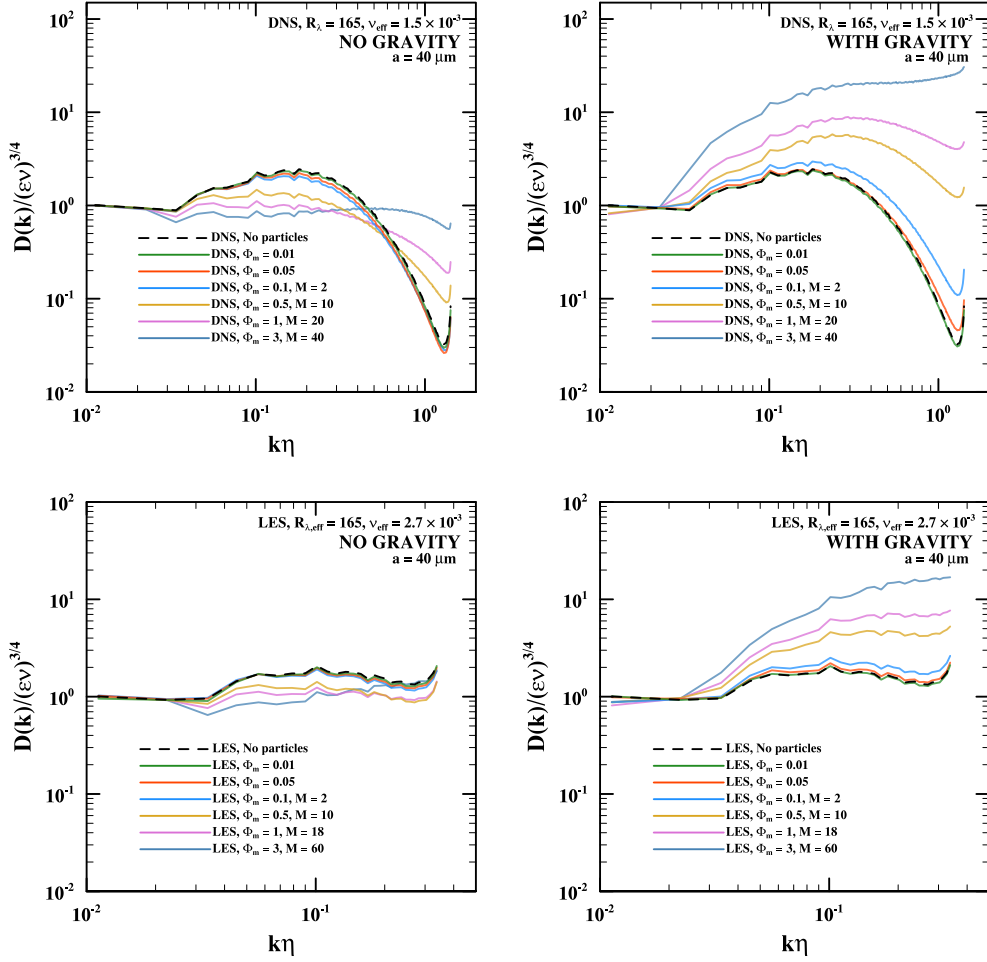
Figure 2.4: The normalised energy dissipation spectra of turbulent flows with droplets of radii 40 μm, with and without gravity, as obtained using both DNS and LES performed under two-way momentum coupling with different particle mass loadings. Dashed lines represent dissipation spectra without turbulence modulation by particles (see Figure 2.2). For comparison (DNS only), see Figure 5 in Rosa et al. (2020).

depending on the particle mass loading and for five different droplet radii, both with and without effects of gravity. These results may be compared with those presented in Rosa et al. (2020, Figure 11 therein), although note that difference in setup and scaling of x-axis is responsible for different outlook of plotted data.

We can easily see that both statistics are increasing with Φ_m for settling particles while in the absence of gravity the effect is opposite. Such trends in u' and ϵ are somewhat expected as both of these statistics are related to the total kinetic energy of turbulence ($u' \propto \sqrt{E}$). In particular, for settling particles the steep increase of both statistics with particle mass loading may be explained by larger fluid velocity gradients caused by fast settling particles. Also note that due to different way of plotting results (relative to Φ_m and not number of particles) it may be observed that u' is much more dependent on radii of individual droplets while ϵ is much less sensitive in that regard and appears to be mainly driven by the particle mass loading of the system. This difference may be seen in results for both DNS and LES.

On that note, again, we can observe qualitative agreement of statistics for both DNS and LES. Same trends can be seen for both methods. When actual magnitudes are concerned,
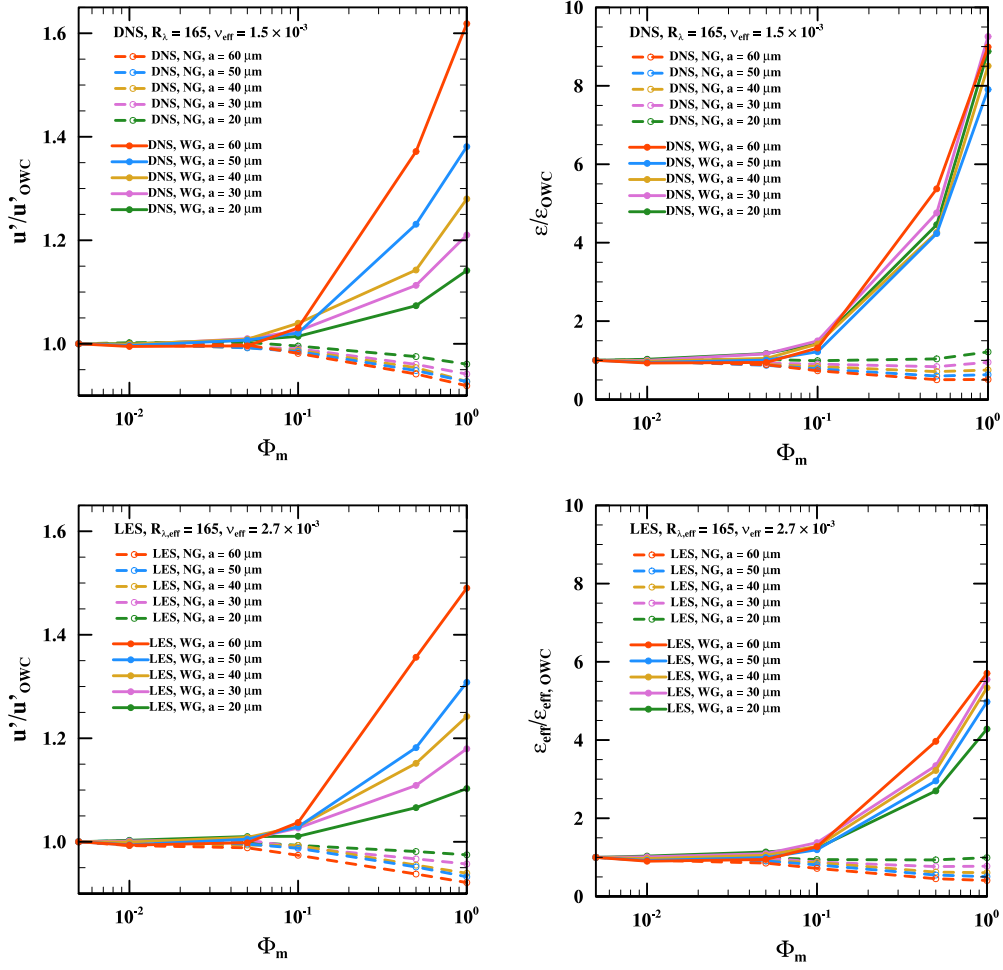
Figure 2.5: Time averaged statistics of turbulent flows as obtained by DNS and LES under two-way momentum coupling, normalised by the corresponding statistics from simulations without turbulence modulation (OWC). Plotted statistics include: the effective energy dissipation rate, ϵ_{eff} (top figures for DNS and LES, respectively), and the RMS fluctuating velocity, u' (bottom figures, likewise). WG denotes simulations with gravity (continuous lines); NG – without gravity (dashed lines). For comparison (DNS only), see Figure 11 in Rosa et al. (2020).

values of u' are surprisingly close for both methods, although slightly underestimated in case of LES. This effect may be due to smaller sensitivity of coarser LES grid to the creation of vortical structures by large inertial particles with high settling velocity which increase the magnitude of turbulence as measured by u'. These vortices are more likely to be induced on smaller scales and subgrid-scale model has no way of picking up such influence.

Much more significant discrepancies can be observed for energy dissipation. In LES the effective values were taken, but they were still approximately two times lower than those for DNS. These differences may be partly explained by the fact that u' does not directly depend on numerical viscosity, while ϵ does and may be affected by inaccuracies in estimating the "effective" viscosity that includes contributions from modelled spectral viscosity. Also inspection of dissipation spectra (and ϵ is defined as its integral) shows that, even though it is consistently adjusted in LES for modes that are directly resolved, dissipation for settling particles is still significantly boosted even for the largest wavenumbers. This increase cannot be fully accounted for in LES by contributions from the subgrid-scale model which is agnostic

of any momentum transfer from particles and is not enough to make up for these unresolved modes.

To sum up these observations, LES shows initial promise in properly representing statistics of background turbulent flow, even when the influence of two-way momentum coupling is considered. Still, it is important to be aware of its limitations and the lack of directly resolved smaller scales that may affect some properties of turbulent flow more than other. Also, it introduces discussion on the quality of chosen subgrid-scale model and whether development of a model that would be sensitive to momentum transfer form particles is viable as a way to alleviate some of observed limitations of LES in this context.

2.2. Kinematic and Dynamic Collision Statistics of Particles

The effects of turbulent flow on certain particles statistics is often more important than properties of the underlying flow itself, whether inherent or modulated by the presence of particles. In atmospheric sciences, for example, modelling of cloud droplets is of paramount importance for better understanding of mechanisms that are involved in precipitation and other phenomena. We may consider single-particle statistics that describe properties of particles that are not directly dependent on other particles in their vicinity, for example the settling velocity of droplets under the effects of gravity. In this study, however, the focus is on two-point particle statistics that measure behaviour of particles in relation with each other. More precisely, we shall explore collisional statistics, i.e. ones that involve particles at contact distance (or, equivalently, when their distance is no larger than sum of their radii). Two of these—the radial distribution function and the radial relative velocity—are introduced in the next section and are commonly referred to as kinematic statistics.

2.2.1. Radial Distribution Function and Radial Relative Velocity

The radial distribution function (RDF) may serve as a measure of preferential concentration of particles. The radial relative velocity (RRV) is a way to quantify average relative velocity of particles. Both of these statistics are important as they may serve to evaluate collision rate of particles in the system. Both were introduced for that very purpose by **Sundaram1997empty citation** and are based on related concepts developed in statistical mechanics.

For monodisperse systems (with fixed particle radius a) the RDF at contact distance (i.e. for $r = R = 2a$) may be effectively computed during simulation using its definition as proposed by **Zhou2001**; Wang et al. (2000). In general, for any distance r from each particle, we consider spherical shell with inner and outer radii equal to $r - \delta r$ and $r + \delta r$, respectively, where δ is a small fraction (~ 0.01) of the contact distance R. Its volume is given by $V_s = 4\pi[(r + \delta)^3 - (r - \delta)^3)]/3$. Also, by N we shall denote the total number of particle pairs, which is equal to $N_{\text{part}}(N_{\text{part}} - 1)/2$, and by N_s the total number of particle pairs detected with their separation distance, r, that fall into spherical shell defined as above. Then, the RDF for distance r at given time t is defined as:

$$g_{11}(r;t) = \frac{N_s/V_s}{N/V}, \tag{2.3}$$

where V is the volume of the entire computational domain. It may be further averaged over time to obtain estimate of $g_{11}(r)$.

To compute the RDF at contact distance, the simplest way would be to just evaluate it for $r = R$. This method, however, was found to be highly susceptible to numerical uncertainties, especially when particle concentration is relatively low. Alternatively, we may use well established fact that for small separation distances ($r < \eta$) function $g_{11}(r)$ follows a power-law dependence with respect to r, with exponent that depends on St and S_V (Rosa et al. 2013, Equation 11 therein). Thus, we may calculate RDF using Equation 2.3 for a range of distances and then fit results into exponential function in order to obtain more accurate estimate of $g_{11}(r = R)$. In practice, similar procedure as in Rosa et al. (2013) was employed. The distances from range between R and $10R$ were divided into 180 discrete bins (shells) used for function fitting by means of least-squares method. In general, for all collision statistics presented in this chapter estimates show that statistical uncertainties do not exceed 3%. Furthermore, it may be noted that for bi- and poly-disperse systems the RDF at contact is close to unity since droplets of different inertia tend to occupy different regions of turbulent flows.
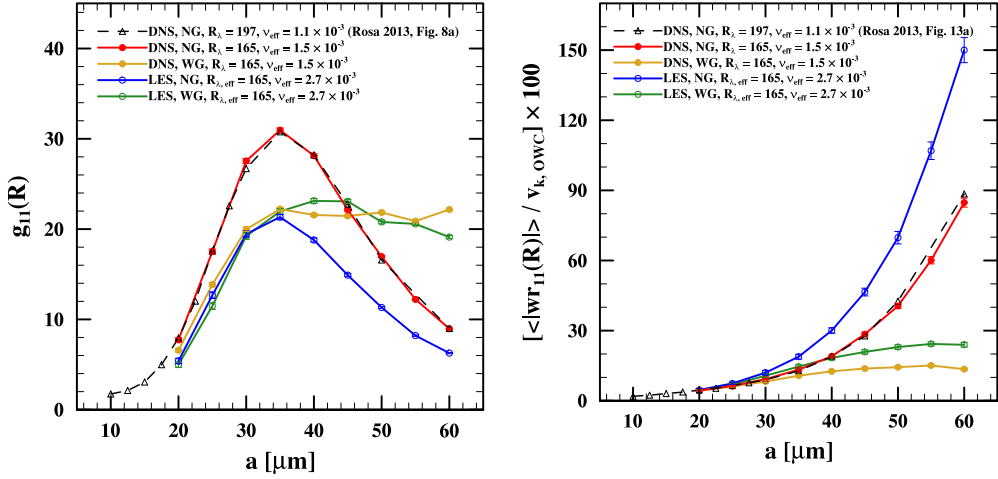

Figure 2.6: The values of the radial distribution function (RDF, left) and the radial relative velocity (RRV, right) at contact distance for simulations under one-way momentum coupling. Results include data from both DNS and LES simulations, with (WG) and without (NG) gravity.

In Figure 2.6 (left) values of the RDF at contact distance obtained from simulations under one-way momentum coupling are shown for both DNS and LES, with and without gravity. For comparison, results for DNS without gravity from Rosa et al. (2013) are shown and perfectly match results obtained in this study. Also they confirm previous observations that clustering of non-settling droplets (as measured by the RDF) is strongest for radii of $30 - 40$ μm, that is whenever the Stokes number is closest to 1. For smaller and larger particles values of the RDF fall off quite rapidly. For much smaller St particle behave more and more as fluid elements and for much larger St they become massive enough to be barely impacted by the fluid, which manifests in much less turbulent clustering. Hence the RDF is expected to approach 1 in those two limits. In case of settling particles, relatively smaller values of the RDF are attained The influence of gravity causes RDF to not drop rapidly for larger particles but remain close to the same peak level attained for particles with $a \approx 35$ μm. This effect is attributed to the tendency of heavier particles to accumulate in the downward flow regions, forming elongated filament-like structures (Rosa et al. 2015).

When gravity is not considered, the results of LES significantly underestimate the RDF, including peak values around $St = 1$ being reduced by approximately 60% (Fede and Simonin

2006; Marchioli et al. 2008; Yang et al. 2008). This difference may be attributed to the filtering of small-scale turbulence which has significant impact on the concentration of particles of that size. On the other hand, LES is confirmed to be much more accurate in predicting the RDF of settling particles (see Rosa and Pozorski 2017). In general, it is argued that heavy settling particles, due to increased velocity in the direction of gravity vector, spend less time interacting with turbulent eddies and more uniformly sample the flow (Ireland et al. 2016). This manifests, in general, in reduced clustering due to turbulence for settling particles and thus lower RDF, irrespective of the method used. This also explains why LES does not lose much accuracy in this case, since filtered scales of turbulence have much less impact on settling particles than those unaffected by gravity.

In case of the relative radial velocity, the method used in its evaluation is similar to the RDF as comparable power-law relation also exists (Rosa et al. 2013, Equation 13 therein). For any two particles with separation vector $\mathbf{r}$ and relative velocity $\mathbf{w}$ we define their radial relative velocity as

$$w_r = \mathbf{w} \cdot \frac{\mathbf{r}}{|\mathbf{r}|}, \tag{2.4}$$

i.e. dot product of relative velocity with direction vector of their separation. Note, that w_r is largest for two particles speeding towards each other. Relative velocities are averaged within shells and fitted into exponential function in a similar fashion as with the RDF. Then, they are averaged over time to obtain $\langle |w_{r,11}(r = R)| \rangle$ and normalised using the Kolmogorov velocity scale, v_k, to make resulting value dimensionless.

Corresponding results of the RRV for simulations under one-way momentum coupling are presented in Figure 2.6 (right). When effects of gravity are not considered the RRV monotonically increases with particle radius and such increase is close to exponential. This is due to increasing contributions from large-scale turbulent motion and other non-local contributions. The picture becomes more complicated for settling particles. We may distinguish regime of light particles (up to 30 μm) where the RRV is independent of the effects of gravity and assumes very similar values to those obtained without accounting for gravity (gravity-independent interaction). This behaviour changes for heavier particles whose settling velocity is larger thus reducing residence time of particles in large-scale turbulent eddies, therefore such accumulation of large-scale motion cannot happen as in case of non-settling particles (gravity-modulated interaction). Also, as previously mentioned, heavier particles tend to arrange into downward-flowing filament-like structures that are characterised by much more velocity correlation, further reducing the RRV. This reduction gets stronger with increasing radius of particles, slowing the increase of RRV until it reaches maximum that depends on R_λ (Rosa et al. 2013) and for flows studied here happens to occur around $a = 50$ μm. Then, further reduction causes the RRV to decrease with particle size, as heavy particles become fast enough to neglect most of the influence of turbulence on their relative velocities.

The results of LES show reverse tendency than for the RDF and they are consistently overestimated by approximately 60% when compared to DNS. This effect may be attributed to the lack of filtered small eddies that introduce more variance in particle motion. In the absence of such disturbances, particles align more with large-scale eddies. Consequently, the effects that cause rapid growth of the RRV with particle size are not only present in LES but are magnified, resulting in the increased RRV. This is still valid for settling particles but similar effects are present as in DNS that reduce the RRV. For that reason, even though overblown in absolute value for LES, the RRV in both methods follows the same trend and the ratio of corresponding values, surprisingly, remains close to constant, especially for $a > 40$ μm.

2.2.2. Dynamic and Kinematic Collision Kernels

The final particle-pair statistic introduced here is the collision kernel defined as the ratio of the number of occurrences of particle collisions to the total number of particle pairs. In general, such kernel is expressed as a symmetric matrix, $\mathbf{\Gamma}(t)$, where entries correspond to ratios of collisions between particles with different properties (usually radii). Here, we consider systems that are monodisperse hence it reduces to single scalar quantity $\Gamma_{11}(t)$. This statistic is of utmost importance, especially in atmospheric sciences, as such ratio of droplet collision affects crucial processes in cloud microphysics, namely droplet collisional growth and coalescence that are driving factors in the formation of precipitation.

The collision kernel may be arduously computed by tracking all collision events in the system and normalising their count by the number of all possible particle pairs. Such value is referred to as the dynamic collision kernel and denoted by $\Gamma_{11}^D(t)$ (or Γ_{11}^D when averaged over time). Statistical uncertainty of such process is calculated as in Rosa et al. (2013, Equation 17 therein). An alternative formulation is the so-called kinematic collision kernel, $\Gamma_{11}^K(t)$, based on **Sundaram1997empty citation**, defined as a function of kinematic statistics introduced in previous section by

$$\Gamma_{11}^K = 2\pi R^2 \langle |w_{r,11}(r = R)| \rangle g_{11}(r = R), \tag{2.5}$$

where r is the separation distance between particles and $R = 2a$. Note that values of both kernels are expected to be in almost perfect agreement (up to statistical uncertainties) and simulation results presented in this study confirm that expectation.
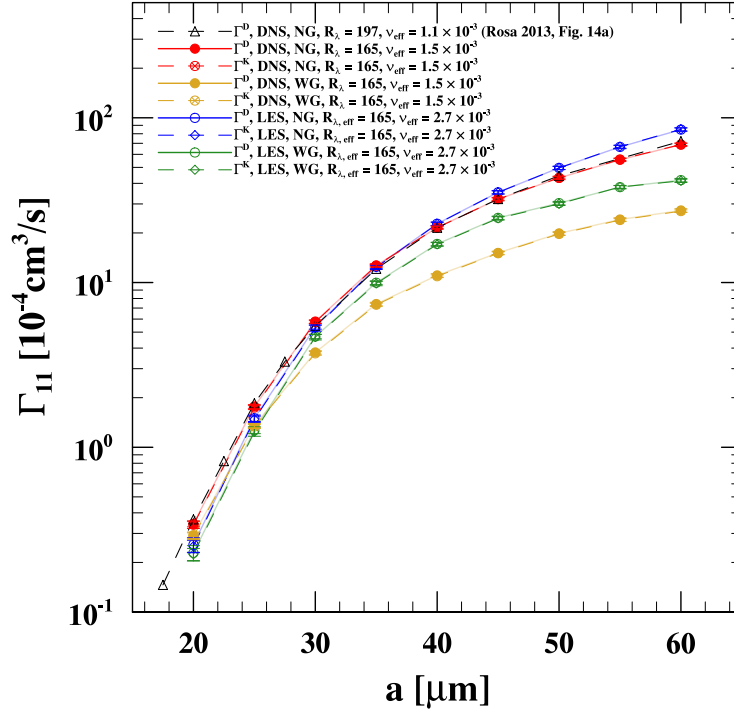

Figure 2.7: The values of both dynamic and kinematic collision kernels for simulations under one-way momentum coupling. Results include data from both DNS and LES simulations, with (WG) and without (NG) gravity. Continuous lines represent values for dynamic kernel (Γ_{11}^D) and dashed ones (almost overlaid on continuous ones due to their close agreement) – for kinematic kernel (Γ_{11}^K).

The values of collision kernels for simulations under one-way momentum coupling are shown in Figure 2.7. The results for dynamic kernel are plotted using continuous lines and

for the kinematic kernel dashed lines are used. The data obtained for DNS confirms previous observations that gravity leads to reduction of collision kernel by the factor of 2 to 3 (Rosa et al. 2013). Based on kinematic formulation, for smaller settling particles ($a < 40$ μm) we may attribute that difference to the lower RDF and for larger ones ($a > 40$ μm) to the rapid growth of the RRV for non-settling particles, at least when compared to reduced relative velocity in gravity-modulated interaction regime. Nonetheless, discrepancies between collision kernels for settling and non-settling particles quickly diminish with smaller radii and for small enough particles ($a < 40$ μm) effects of gravity on Γ_{11} may be considered negligible.

The comparison of DNS and LES results depends on whether we include gravity. When gravity is not considered collision kernels provided by DNS and LES are in quantitative agreement. This may be explained by the values of the RDF and the RRV that are, respectively, underestimated or overestimated by approximately the same relative amount. This is due to filtering of small-scales eddies that increase turbulent concentration but also make large-scale flow motion of fluid more prominent increasing the RRV. These two effects seem to cancel each other when the particle collision rate is question, bringing values obtained by both methods close to each other. Different picture presents itself for settling particles. For smaller particles ($a < 30$ μm) both DNS and LES are in quite good agreement. For smallest considered radii LES even tends to overestimate the collision kernel as the RDF is similar and the RRV is slightly overestimated in LES. Nonetheless, absolute differences of Γ_{11} are rather negligible for such low inertia particles.

On the other hand, for particles with radii larger than 30 μm the difference between DNS and LES grows significantly. This may be explained by the fact that LES correctly predicts the RDF for more massive particles while still overestimates the RRV as in case of smaller droplets. This leads to similar difference in Γ_{11} as in the RRV and no cancellation occurs as for particles unaffected by gravity. The closer inspection of the RDF for LES with gravity shows that it may consistently decrease for particles with $a > 50$ μm but such claim cannot be confirmed by available data and results of previous studies (Rosa and Pozorski 2017) suggest that it is quite unlikely. But if that is so, such reduction of LES inaccuracy may eventually happen for particles that are massive enough. Moreover, it may be observed that difference between LES and DNS starts to diminish when $a = 60$ μm. Still, such discrepancy in prediction of collision rate of larger settling particles between DNS and LES is considerable and should be further investigated.

2.2.3. Collision Statistics in Simulations under Two-Way Momentum Coupling

In previous sections basic notions of collisional particle statistics were introduced, as well as methods of their computation backed by a reproduction of already established results for simulations under one-way momentum coupling. Here, estimates of these statistics using simulations under two-way momentum coupling shall be presented. Such results were recently presented and systematically analysed for DNS by Rosa et al. (2020, 2022), yet no such study were performed using LES. For that reason the focus here is on results obtained by LES and their comparison with those coming from DNS.

The results are presented for both kinematic statistics (RDF, RRV) and collision kernels. Note that values of both dynamic and kinematic kernels were confirmed to be in quantitative agreement within statistical uncertainty, hence only data for dynamic kernel is explicitly shown. Three types of plots are used to showcase influence of two-way momentum coupling on these statistics. Firstly, they are plotted for selected fixed values of Φ_m depending on particle radii (see Figures 2.8, 2.10, and 2.12; top row). These may be considered an extension

of plots from Sections 2.2.1 and 2.2.2 since they also contain similar curves shown for OWC simulations and extended by additional ones that involve TWC with increasing mass loading. Remaining plots show droplet statistics for two specific radii, 30 μm and 40 μm, that were chosen to represent particles most affected by turbulence (i.e. with $St \sim 1$), as a function of the number of particles in the system. Plots in the bottom row of Figures 2.8, 2.10, and 2.12 are limited to relatively small particle content (up to 20 million; equivalent to $\Phi_m \approx 0.15$ for $a = 40$ μm). The values obtained from OWC simulations are included for reference on the leftmost edge of the plot (i.e. 0 on the x-axis). Results from simulations with broader range of mass loadings are shown in Figures 2.8, 2.10, and 2.12. Simulations where super-particle parameterisation was used (i.e. $M > 1$) are explicitly marked by dashed line. For more information pertaining to simulations with super-particle parameterisation and what exact values of M were used, see Appendix C. Results without effects of gravity are shown on the left, and those for settling particles - on the right.

Radial Distribution Function (RDF)

Figures 2.8 and 2.9 show results for the RDF. The RDF for non-settling particles clearly exhibits similar dependence on particle size as in case of OWC but its absolute value is being reduced with the increase of mass loading. When effects of gravity are considered the RDF is generally boosted in TWC for the smallest range of particles (~ 20 μm), while it becomes smaller with increasing particle radius and mass loading, reaching a plateau for heavier particles. These results for DNS are confirmed by Rosa et al. (2020, Fig. 19), where dependence on particle size more easily appreciable since results were obtained for a broader range of droplet radii. Here, however, data is extended with plots for larger mass loadings (0.5, 1) that were not included in previous studies.

The results of LES for non-settling particles are consistent with those of DNS in terms of general trends, in particular the significant reduction of the RDF that is consistents with results of OWC simulations. As observed in Rosa et al. (2020), the RDF is barely sensitive to TWC and larger mass loadings (even as large as $\Phi_m = 1$, shown here) for both very small (20 μm) and very large particles (60 μm). It is so, because low-inertia particles have little impact on turbulence modulation and their behaviour in dominated by the fluid flow, while heavy particles are not very sensitive to influence of turbulence in general and turbulence modulated by other particles in particular. The same conclusion is valid for the results of LES. One interesting difference is the fact that results of LES are much less influenced by increasing mass loading. For $\Phi_m \leq 0.1$ mass loading seems to have very little effect on the RDF. When number of number of particles is much larger ($\Phi_m = 0.5, 1$) the effects are more pronounced, but still values estimatd by LES remain larger than those for DNS. As shown before (see Section 2.1.4) the large amount of heavy particles has tendency to weaken turbulence when gravity is neglected, which may result in reduced particle clustering. In LES, smallest turbulent scales are parameterised by subgrid-scale model which is agnostic to any momentum transfer from particles to fluid, hence such dampening of smallest fluctuations cannot happen. This may explain that, up to a point, LES is not as sensitive to the increasing mass loadings in TWC. Still, for large enough Φ_m, even larger turbulent scales that are directly resolved in LES may be affected, although this reduction is not as dramatic as in DNS.

When settling particles are considered the results for LES do not follow those for DNS as closely as was in case of OWC simulations. Still, estimates given by LES follow similar pattern of initial (for $a \approx 20$ μm) strengthening of clustering compared to OWC, then followed by gradual increase ending in plateau for heavier particles. Moreover, we observe that results of DNS and LES tend to converge for heavier particles (60 μm). Also, similarly to DNS, in
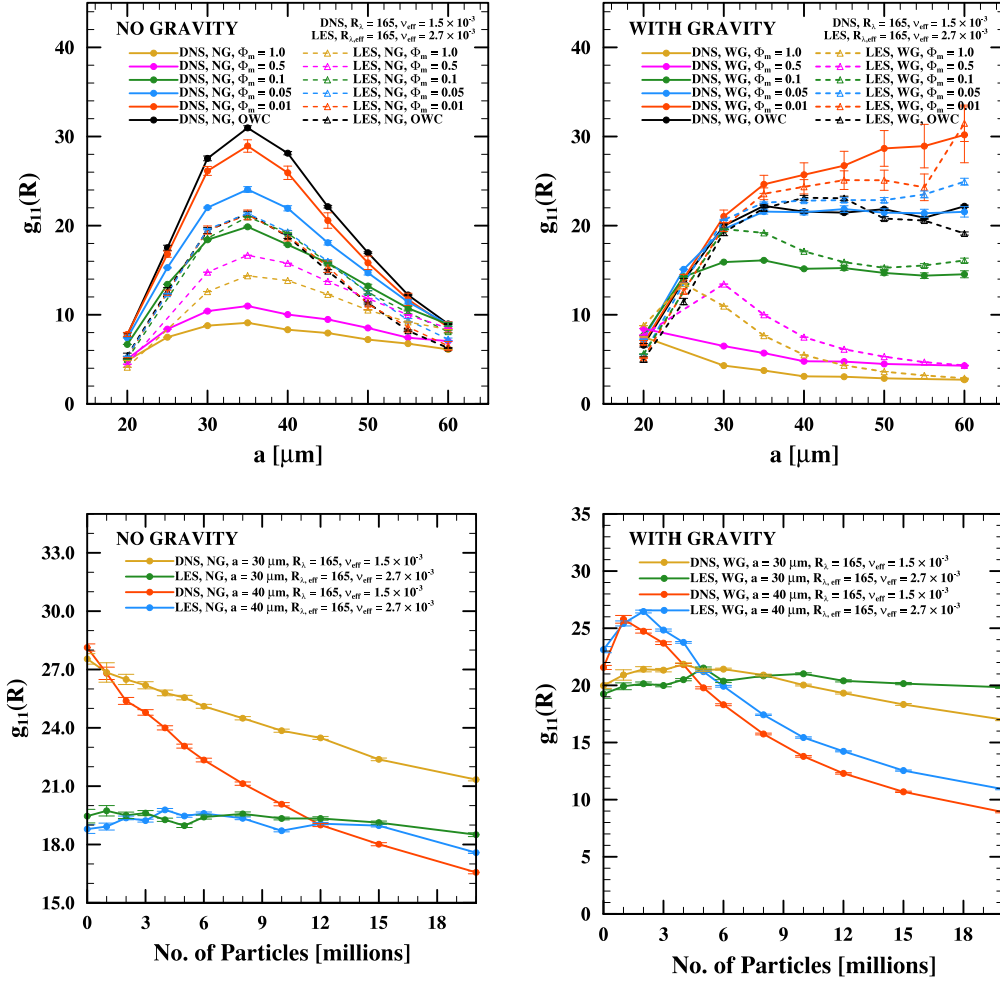
Figure 2.8: The values of radial distribution function (RDF) at contact distance for simulations under two-way momentum coupling using both DNS and LES. Top plots show relation of RDF on particle radius for several fixed values of mass loading, Φ_m (also compared with results for OWC). Bottom ones show the dependence of RDF on the number of particles (in millions) for particles with radii 30 µm and 40 µm. Plots on the left show results without effects of gravity (NG), and those on the right consider settling particles (WG).

TWC simulations with small mass loading ($\Phi_m \sim 0.01$), the RDF in LES is also larger than obtained by OWC for the entire considered range of radii.

When the dependence of the RDF on the number of particles is analysed there are clear differences between cases for settling and non-settling particles. When gravity is neglected the RDF decreases monotonically with mass loading. In simulations with gravity, however, initial increase and peak is observed that subsequently turns into monotonic decrease for larger mass loadings. The prominence and position of such peak depends on the particle radius.

Interestingly, as in the case of OWC (see Figure 2.6), the results obtained by LES are much more aligned with DNS when gravity is condidered. For non-settling particles the RDF remains close to constant and almost completely insensitive to the increase in mass loading. It is necessary to look at a larger picture (Figure 2.9) to notice that results from LES become sensitive to Φ_m at higher loadings (~ 0.3) where they start to gradually decrease. This is
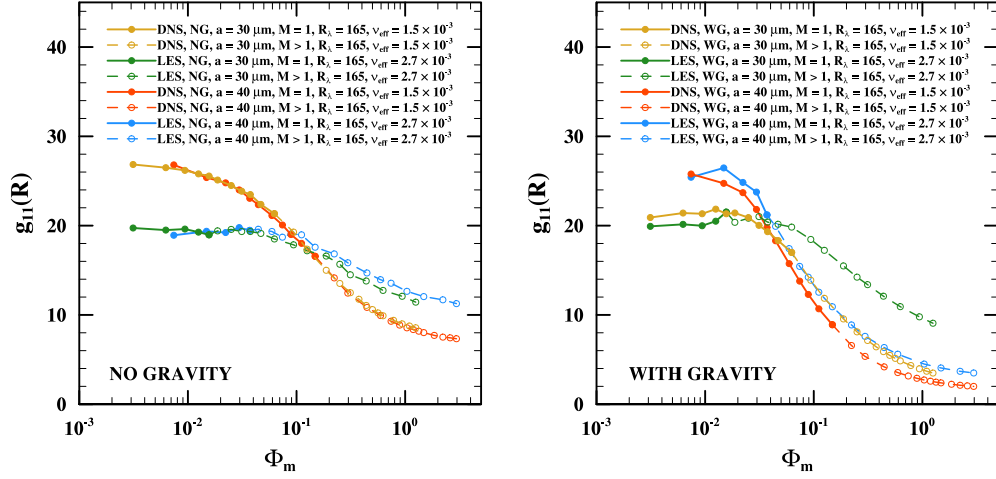
Figure 2.9: The values of RDF for wider range of mass loadings. It may be considered as an extension of bottom plots from Figure 2.8 where scope was limited to 20 million particles ($\Phi_m \approx 0.1$). Here, results include wider range of mass loadings where TWC should be most prominent (i.e. around 0.1 to 1) and where it may even not be sufficient (i.e. four-way coupling regime for $\Phi_m > 1$). Continuous lines represent simulations without super-particle parameterisation ($M = 1$), while dashed ones show where super-particle parameterisation was necessary to obtain larger mass loadings. For precise information on values of M for each simulation, see Appendix C.

consistent with previous observations and proposed explanation.

When settling particles are considered the results of LES seem to follow those from DNS more closely. In general, there is some overestimation on part of LES but for the most part it remains relatively small. These discrepancies seem to be more significant for lighter particles since they are more susceptible to TWC-agnostic turbulence from subgrid-scale model and less capable of turbulence modulation due to filtering of small-scale turbulence. For heavier particles (40 μm) these differences are smaller in absolute value and exhibited amount of over-prediction is consistent throughout the entire range of considered mass loadings. Moreover, based on data from Figure 2.8 (top right), it is expected that for larger particles ($a \geq 60$ μm) results for DNS and LES should become more and more aligned.

As a side note, Figure 2.9 is a great opportunity to showcase different regimes that depend on the amount of particles in the system. Firstly, we have the one-way coupling regime, which is approximately defined for mass loadings smaller than 0.1 and where TWC is not considered necessary to accurately model the system. As pointed out by Rosa et al. (2020), even in this regime inclusion of TWC may provide physically significant adjustments. This may be clearly seen in the plot where the RDF depends on mass loading and starts to decrease much earlier than for $\Phi_m = 0.1$. Note that this regime threshold is also affected by using LES. It is due to the filtering of small-scale structures and it delays the effects of TWC that start showing up when $\Phi_m \sim 0.2$. Then, for $0.1 < \Phi_m < 1$ we have the two-way coupling regime, where effects of TWC are most visible and necessary for physical fidelity. This range of mass loadings is characterised by the steepest decrease in the RDF as it is most sensitive to additional effects resolved due to two-way momentum coupling. Finally, when Φ_m exceeds 1 we say that such systems belong to the four-way coupling regime, where TWC becomes insufficient and to correctly account for physics of such systems it is necessary to directly resolve interactions between particles. This threshold may be witnessed on the plot as the values of the RDF for this range of mass loadings start to plateau. It means that TWC is not enough to entirely

grasp complexity of a system that is such densely packed with dispersed phase.

Radial Relative Velocity (RRV)

Figures 2.10 and 2.11 show radial relative velocities obtained from two-way coupled DNS and LES. When DNS is considered, for smaller values of Φ_m not exceeding 0.1, dependence of the RRV on particle sizes confirms results of Rosa et al. (2020, Fig. 22 therein). For non-settling particles we observe only slight increase in the relative velocities with growing Φ_m for particles of intermediate radii ($30 - 50$ μm). This effect is direct consequence of two-way momentum coupling and is attributed to the transfer of momentum from particles to fluid that increases its local velocity and, in turn, affects neighbouring particles by further decorrelating their motion. For settling particles, as expected, relatively large increase in the RRV is observed with growing particle inertia and mass loadings. It is caused by strong modulation of turbulent flow by fast settling particles that create small-scale vortical structures with high angular momentum that highly impact relative motion of all particles. The results for larger mass loadings, i.e. 0.5 and larger that were not included in Rosa et al. (2020), are showing even stronger increase in the RRV for both settling and non-settling particles. In Figure 2.10 (top right) lines for $\Phi_m = 1$ are not shown, since for $a = 60$ μm the RRV reaches normalised values of $5.19\,v_{k,\,\mathrm{OWC}}$ for DNS and $4.86\,v_{k,\,\mathrm{OWC}}$ for LES. This shows that effects described above are very strongly amplified as Φ_m rises.

The results of LES for non-settling particles show an important inversion of trend, as the effect of TWC (getting stronger with Φ_m) is the relative decline in values of the RRV compared to OWC. Also effects of TWC are still visible and getting more pronounced for high inertia particles (60 μm), while in DNS particles of sizes around 55 μm (Rosa et al. 2020, Fig. 22a therein) are unaffected by TWC. In Section 2.2.1 a relatively high overestimation of the RRV in LES (OWC) was explained by filtering of small-scales of turbulence, thus eliminating decorrelating effects at these scales. Inclusion of TWC cannot affect this directly as subgrid-scale model is agnostic to any momentum transfer from particles to fluid. This influence of TWC on results for LES needs further investigation to explain this complex mechanism.

In case of particles affected by gravity the results are much more familiar (except already observed peculiar behaviour of the RRV for high mass loadings when $\Phi_m \geq 0.5$). We may observe that relative velocities from LES follow similar trend as for DNS. Here, increase of the RRV is not only attributable to extra turbulent structures induced by fast settling particles but also to the filtering of small-scale turbulence. Thus, LES has tendency to overestimate DNS results, especially for heavy droplets (40 μm and larger). With the increase of mass loading such overestimation becomes smaller and for some range of smaller particles (depending on Φ_m) the RRV in LES becomes underestimated. This is because larger number of particles escalates turbulence modulation due to TWC effects that become dominant. This influence, however, is stronger in DNS as also small scale turbulence is induced this way and not filtered as in LES. For that reason such overestimation happens for lighter particles as they are more susceptible to the turbulence induced at smaller scales.

The effects of increasing mass loading on the RRV are opposite to those for the RDF and relative velocities increase with larger numbers of particles in the system (Rosa et al. 2020, Fig. 23 and 24 therein). This increase is only slight or close to none without gravity, but for particles affected by gravity it is much more dramatic, which can be explained by heavy turbulence modulation due to settling particles. When LES is considered a similar pattern may be recognised as for the RDF. For non-settling particles and small enough mass loadings ($\Phi_m < 0.2$) the RRV is virtually constant and shows no signs of being affected by the number of particles in the system. Again, this is due to the filtering of small-scale turbulence which is limiting the effects of turbulence modulation in TWC. This effect becomes significant only
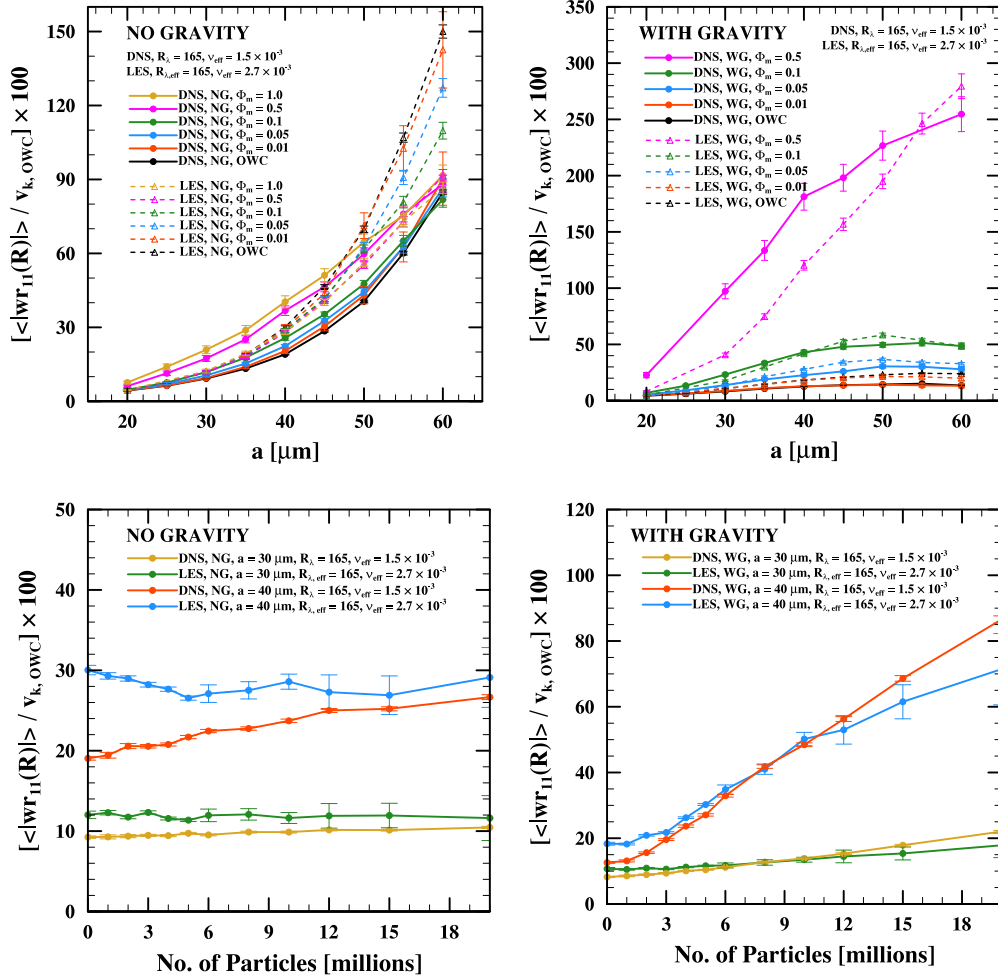
Figure 2.10: The values of radial relative velocity (RRV) at contact distance for simulations under two-way momentum coupling using both DNS and LES. Consistent with Figure 2.8.

for larger mass loadings, when intermediate scales can be affected due to larger concentration of particles. In general, statistics obtained by LES quite closely follow those from DNS, especially in the case of settling particles. Furthermore, as with the RDF, the quality of prediction improves for more massive particles.

Collision Kernel

Finally, the results concerning the (dynamic) collision kernel are shown in Figures 2.12 and 2.13. In simulations without gravity collision kernels show very little sensitivity to the effects of TWC. Still, a slight decrease of Γ_{11}^D is observed when mass loading is increasing. This may be attributed to the fact that with growing number of particles the RDF is getting smaller, or—equivalently—distribution of particles in the system becomes more uniform. Results obtained by LES are quite aligned with those from DNS and similar trends may be discerned as for OWC (see Section 2.2.2). LES underestimates collision rate for smaller particles (up to 30 μm) but overestimates it for those with larger radii. The latter is mainly due to higher values of the RRV in LES, but with TWC this discrepancy is reduced as the overestimation of radial velocity by LES becomes smaller with increasing Φ_m. On the other hand, for larger mass loadings the RDF is much smaller in DNS than in LES. It makes difference in Γ_{11}^D between OWC and high-Φ_m TWC even larger. Thus, for larger particles (50 − 60 μm) the
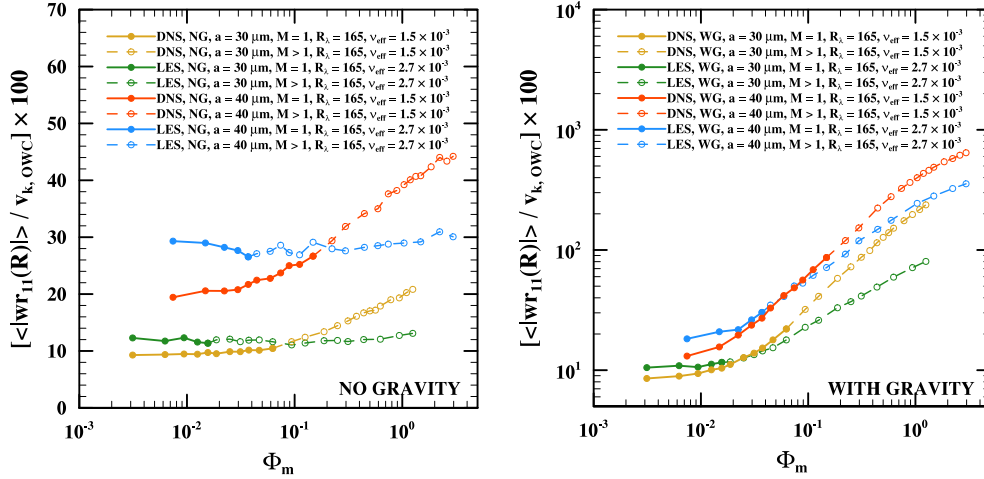
Figure 2.11: The values of RRV for wider range of mass loadings. Consistent with Figure 2.9.

overprediction of collision kernel by LES is increased. Furthermore, since both the RDF and the RRV are unaffected by changes in mass loading until it reaches certain threshold (for $\Phi_m \sim 0.2$, exact value depends on particle size), the same is true for collision kernel. Nonetheless, very crowded lines in Figure 2.12 (top left) are sign of a limited sensitivity of the collision rate to the effects of TWC and varying mass loading, as well as method used to obtain results (DNS or LES).

Results for settling particles show much more spread that indicates greater impact of TWC on collision rate in that case. First of all, the general trend is opposite to that observed for particles unaffected by gravity. The collision kernel is monotonically increasing with particle mass loading due to stronger effects of turbulence modulation that lead to more clustering and higher relative velocities. For LES, a similar phenomenon may be seen as for non-settling particles, where LES underpredicts collision kernel for smaller particles and overpredicts it for larger ones. Also, as particles become heavier, the magnitude of such overshot decreases. More importantly, we can observe that difference between DNS and LES becomes smaller and smaller as Φ_m increases. In edge case, for $\Phi_m = 1$ and particles with radius 40 μm or larger the results from both DNS and LES are in perfect agreement. On the flip side, the worst discrepancies between two methods also happen for large mass loadings ($\Phi_m \geq 0.5$) but for particles on the smaller side of the range considered (especially for $a = 20$ μm). This is effect of underprediction of the RRV by LES for simulations with large amounts of lighter particles that are susceptible to small-scale turbulence induced in DNS that cannot be reproduced by LES due to filtering of smallest scales of turbulence.

When we analyse dependence of Γ_{11}^D on the amount of particles, again, we can see that behaviour is different for non-settling and settling particles. For the former, the collision kernel slightly decreases, while for the latter we can observe more definite increase in collision rate with increasing mass loading. The collision kernel estimated by LES is in relatively good agreement with results obtained by DNS and discrepancies seem to diminish with increasing mass loading of the dispersed phase. What is interesting, even though kinematic statistics obtaied by DNS and LES were more aligned for particles of larger radius, 40 μm in particular, for collision kernel the reverse is true. Results for $a = 40$ μm are well aligned, but in case of $a = 30$ μm we observe almost perfect agreement between two methods for both small and large mass loadings. This may be attributed to the cancellation of certain effects on kinematic statistics specific to LES, in particular ones that arise from filtering of small scales
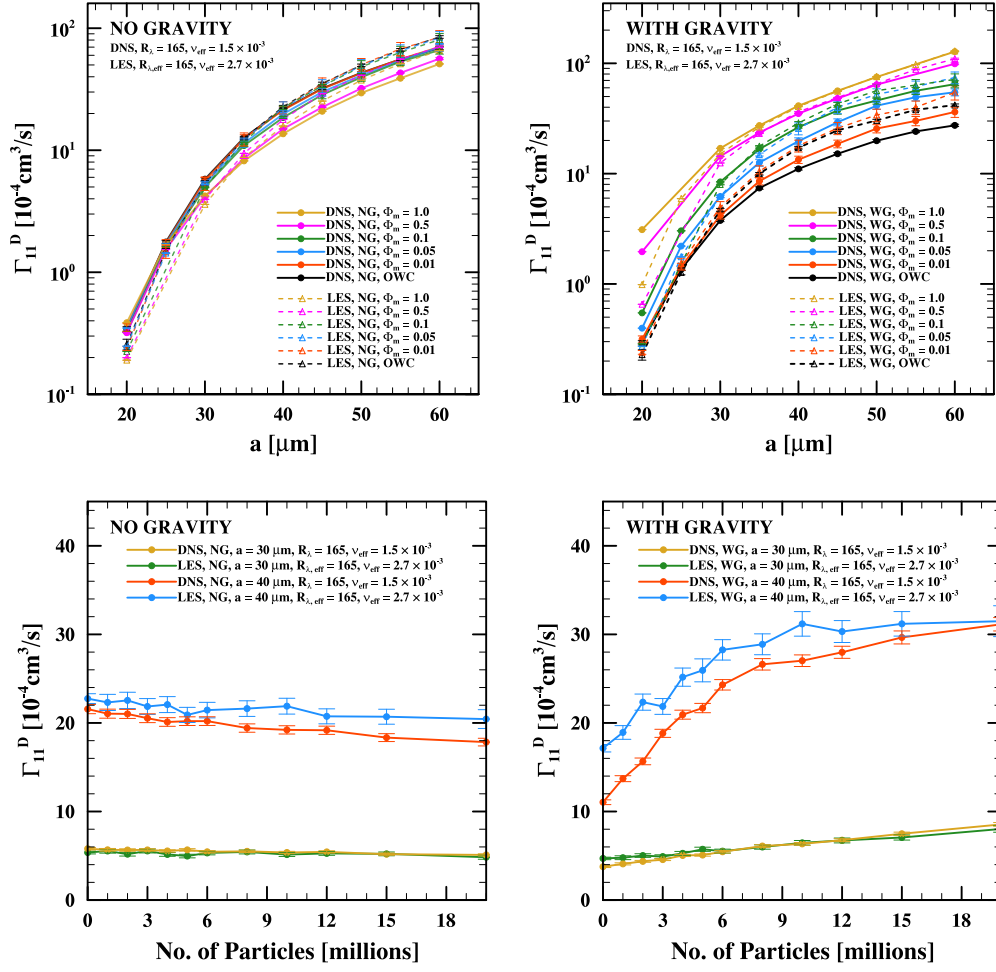
Figure 2.12: The values of dynamic collision kernel (Γ_{11}^D) for simulations under two-way momentum coupling using both DNS and LES. Consistent with Figure 2.8.

of turbulence and cause underestimation of the RDF and overestimation of the RRV.
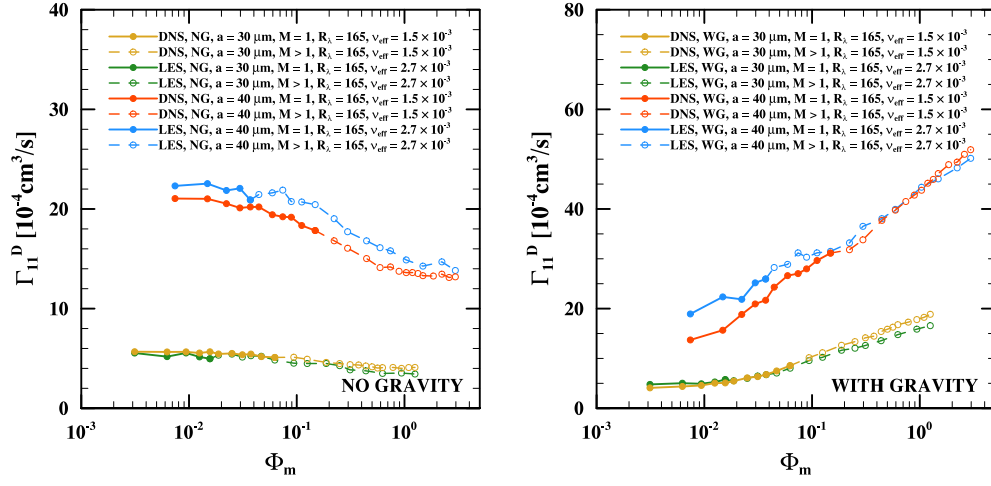
Figure 2.13: The values of dynamic collision kernel for wider range of mass loadings. Consistent with Figure 2.9.

Chapter 3

Comparison of DNS and LES Performance

NNN

Conclusions

NNN

Appendix A

Pseudo-Spectral Method in Detail

NNN

Appendix B

Effects of Subgrid-Scale Model on Flow Statistics

NNN

Appendix C

Super-Particle Parametrisations in Simulations under Two-Way Momentum Coupling

NNN

References

Ababaei, A., B. Rosa, J. Pozorski, and L.-P. Wang (2021). "On the effect of lubrication forces on the collision statistics of cloud droplets in homogeneous isotropic turbulence". In: *Journal of Fluid Mechanics* 918, A22.

Allen, M. P. and T. J. Tildesley (1987). *Computer Simulation of Liquids*. Oxford University Press.

Arabas, S. and S.-I. Shima (2013). "Large-Eddy Simulations of Trade Wind Cumuli Using Particle-Based Microphysics with Monte Carlo Coalescence". In: *Journal of the Atmospheric Sciences* 70 (9), pp. 2768–2777.

Ayala, O., W. W. Grabowski, and L.-P. Wang (2007). "A hybrid approach for simulating turbulent collisions of hydrodynamically-interacting particles". In: *Journal of Computational Physics* 225 (1), pp. 51–73.

Ayala, O., B. Rosa, L.-P. Wang, and W. W. Grabowski (2008). "Effects of turbulence on the geometric collision rate of sedimenting droplets. Part 1. Results from direct numerical simulation". In: *New Journal of Physics* 10, 075015.

Ayala, O. and L.-P. Wang (2013). "Parallel implementation and scalability analysis of 3D Fast Fourier Transform using 2D domain decomposition". In: *Parallel Computing* 39 (1), pp. 58–77.

Ayala, O., H. Parishani, L. Chen, B. Rosa, and L.-P. Wang (2014). "DNS of hydrodynamically interacting droplets in turbulent clouds: Parallel implementation and scalability analysis using 2D domain decomposition". In: *Computer Physics Communication* 185, pp. 3269–3290.

Balachandar, S. (2009). "A scaling analysis for point-particle approaches to turbulent multiphase flows". In: *International Journal of Multiphase Flow* 35 (9), pp. 801–810.

Balachandar, S. and J. K. Eaton (2010). "Turbulent Dispersed Multiphase Flows". In: *Annual Review of Fluid Mechanics* 42 (1), pp. 111–133.

Bosse, T., L. Kleiser, and E. Meiburg (2006). "Small particles in homogeneous turbulence: Settling velocity enchancement by two-way coupling". In: *Physics of Fluids* 18, 027102.

Brauner, N. (2003). "Liquid-Liquid Two-Phase Flow Systems". In: *Modelling and Experimentation in Two-Phase Flow*. Ed. by V. Bertola. Wien: Springer–Verlag, pp. 221–279.

Buaria, D., A. Pumir, E. Bodenschatz, and P. K. Yeung (2019). "Extreme velocity gradients in turbulent flows". In: *New Journal of Physics* 21, 043004.

Buaria, D., E. Bodenschatz, and A. Pumir (2020). "Vortex stretching and enstrophy production in high Reynolds number turbulence". In: *Physical Review Fluids* 5, 104602.

Chollet, J.-P. and M. Lesieur (1981). "Parameterization of Small Scales of Three-Dimensional Isotropic Turbulence Utilizing Spectral Closures". In: *Journal of the Atmospheric Sciences* 38 (12), pp. 2747–2757.

Crowe, C. T., J. D. Schwarzkopf, M. Sommerfeld, and Y. Tsuji (2012). *Multiphase Flows with Droplets and Particles*. 2nd ed. CRC Press.

Devenish, B. J. et al. (2012). "Droplet growth in warm turbulent clouds". In: *Quarterly Journal of the Royal Meteorological Society* 138 (667), pp. 1401–1429.

Dmitruk, P., L.-P. Wang, W. H. Matthaeus, R. Zhang, and D. Seckel (2001). "Scalable parallel FFT for spectral simulations on a Beowulf cluster". In: *Parallel Computing* 27, pp. 1921–1936.

Doms, G. and M. Baldauf (2021). *A Description of the Nonhydrostatic Regional COSMO-Model. Part I: Dynamics and Numerics*. URL: https://www.cosmo-model.org/content/model/documentation/core/default.htm (visited on 06/22/2022).

Elghobashi, S. (1994). "On Predicting Particle-Laden Turbulent Flows". In: *Applied Scientific Research* 52, pp. 309–329.

Elghobashi, S. and G. C. Truesdell (1993). "On the two-way interaction between homogeneous turbulence and dispersed solid particles. I: Turbulence modification". In: *Physics of Fluids A: Fluid Dynamics* 5 (7), pp. 1790–1801.

Ernst, M., M. Sommerfeld, and S. Lain (2019). "Quantification of preferential concentration of colliding particles in a homogenous isotropic turbulent flow". In: *International Journal of Multiphase Flow* 117, pp. 163–181.

Eswaran, V. and S. B. Pope (1988). "An examination of forcing in direct numerical simulations of turbulence". In: *Computers and Fluids* 16 (3), pp. 257–278.

Fede, P. and O. Simonin (2006). "Numerical study of the subgrid fluid turbulence effects on the statistics of heavy colliding particles". In: *Physics of Fluids* 18, 045103 (4).

Ferziger, J. H., M. Perić, and R. L. Street (2020). *Computational Methods for Fluid Dynamics*. 4th ed. Springer.

Garg, R., C. Narayanan, D. Lakehal, and S. Subramaniam (2007). "Accurate numerical estimation of interphase momentum transfer in Lagrangian-Eulerian simulations of dispersed two-phase flows". In: *International Journal of Multiphase Flow* 33 (12), pp. 1337–1364.

Garg, R., C. Narayanan, and S. Subramaniam (2009). "A numerically convergent Lagrangian-Eulerian simulation method for dispersed two-phase flows". In: *International Journal of Multiphase Flow* 35, pp. 376–388.

Gore, R. A. and C. T. Crowe (1989). "Effect of particle size on modulating turbulent intensity". In: *International Journal of Multiphase Flow* 15 (2), pp. 279–285.

Grabowski, W. W. and L.-P. Wang (2013). "Growth of Cloud Droplets in a Turbulent Environment". In: *Annual Review of Fluid Mechanics* 45 (1), pp. 293–324.

Guichard, F. and F. Couvreux (2017). "A short review of numerical cloud-resolving models". In: *Tellus A: Dynamic Meteorology and Oceanography* 69, 1373578 (1).

Ireland, P. J., A. D. Bragg, and L. R. Collins (2016). "The effect of Reynolds number on inertial particle dynamics in isotropic turbulence. Part 2. Simulations with gravitational effects". In: *Journal of Fluid Mechanics* 796, pp. 659–711.

Jin, G., G.-W. He, and L.-P. Wang (2010). "Large-eddy simulation of turbulent collision of heavy particles in isotropic turbulence". In: *Physics of Fluids* 22, 055106 (5).

Lain, S., M. Ernst, and M. Sommerfeld (2020). "Study of Colliding Particle-Pair Velocity Correlation in Homogeneous Isotropic Turbulence". In: *Applied Sciences* 10, 9095.

Marchioli, C., M. V. Salvetti, and A. Soldati (2008). "Some issues concerning large-eddy simulation of inertial particle dispersion in turbulent bounded flows". In: *Physics of Fluids* 20, 040603 (4).

Matsuda, K., K. Schneider, and K. Yoshimatsu (2021). "Scale-dependent statistics of inertial particle distribution in high Reynolds number turbulence". In: *Physical Review Fluids* 6, 064304.

Maxey, M. R. and J. J. Riley (1983). "Equation of motion for a small rigid sphere in nonuniform flow". In: *Physics of Fluids* 26 (4), pp. 883–889.

Monchaux, R. and A. Dejoan (2017). "Settling velocity and preferential concentration of heavy particles under two-way coupling effects in homogeneous turbulence". In: *Physical Review Fluids* 2, 104302.

Morrison, H. et al. (2020). "Confronting the Challenge of Modeling Cloud and Precipitation Microphysics". In: *Journal of Advances in Modeling Earth Systems* 12, e2019MS001689 (8).

Onishi, R., K. Takahashi, and J. C. Vassilicos (2013). "An efficient parallel simulation of interacting inertial particles in homogeneous isotropic turbulence". In: *Journal of Computational Physics* 242, pp. 809–827.

Orszag, S. a. and G. S. Patterson (1972). "Numerical Simulation of Three-Dimensionsl Homogeneous Isotropic Turbulence". In: *Physical Review Letters* 28 (2), pp. 76–79.

Parishani, H., O. Ayala, B. Rosa, L.-P. Wang, and W. W. Grabowski (2015). "Effects of gravity on the acceleration and pair statistics of inertial particles in homogeneous isotropic turbulence". In: *Physics of Fluids* 27, 033304.

Peng, Y., W. Liao, L.-S. Luo, and L.-P. Wang (2009). "A Comparative Study of the Lattice Boltzmann and Pseudo-Spectral Methods for Decaying Homogeneous Isotropic Turbulence". In: *47th AIAA Aerospace Sciences Meeting*, Paper 587.

Pope, S. B. (2000). *Turbulent Flows.* Cambridge: Cambridge university Press.

Pozorski, J. and S. V. Apte (2009). "Filtered particle tracking in isotropic turbulence and stochastic modelling of subgrid-scale dispersion". In: *International Journal of Multiphase Flow* 35, pp. 118–128.

Rosa, B., H. Parishani, O. Ayala, L.-P. Wang, and W. W. Grabowski (2011). "Kinematic and dynamic pair collision statistics of sedimenting inertial particles relevant to warm rain initiation". In: *Journal of Physics: Conference Series* 318, 072016 (7).

Rosa, B., H. Parishani, O. Ayala, W. W. Grabowski, and L.-P. Wang (2013). "Kinematic and dynamic collision statistics of cloud droplets from high-resolution simulations". In: *New Journal of Physics* 15, 045032.

Rosa, B., H. Parishani, O. Ayala, and L.-P. Wang (2015). "Effects of forcing time scale on the simulated turbulent flows and turbulent collision statistics of inertial particles". In: *Physics of Fluids* 27, 015105.

— (2016). "Settling velocity of small inertial particles in homogeneous isotropic turbulence from high-resolution DNS". In: *International Journal of Multiphase Flow* 83, pp. 217–231.

Rosa, B. and J. Pozorski (2017). "Impact of subgrid fluid turbulence on inertial particles subject to gravity". In: *Journal of Turbulence* 18 (7), pp. 634–652.

Rosa, B., J. Pozorski, and L.-P. Wang (2020). "Effects of turbulence modulation and gravity on particle collision statistics". In: *International Journal of Multiphase Flow* 129, 103334.

Rosa, B., S. Kopeć, A. Ababaei, and J. Pozorski (2022). "Collision statistics and settling velocity of inertial particles in homogeneous turbulence from high-resolution DNS under two-way momentum coupling". In: *International Journal of Multiphase Flow* 148, 103906.

Squires, K. D. and J. K. Eaton (1990). "Particle response and turbulence modification in isotropic turbulence". In: *Physics of Fluids A: Fluid Dynamics* 2 (7), pp. 1191–1203.

Sullivan, N. P., S. Mahalingam, and R. M. Kerr (1994). "Deterministic forcing of homogeneous, isotropic turbulence". In: *Physics of Fluids* 6, 1612.

Tom, J. and A. D. Bragg (2019). "Multiscale preferential sweeping of particles settling in turbulence". In: *Journal of Fluid Mechanics* 871, pp. 244–270.

Wang, L.-P. and M. R. Maxey (1993). "Settling velocity and concentration distribution of heavy particles in homogeneous isotropic turbulence". In: *Journal of Fluid Mechanics* 256, pp. 27–68.

Wang, L.-P., A. S. Wexler, and Y. Zhou (2000). "Statistical mechanical description and modelling of turbulent collision of inertial particles". In: *Journal of Fluid Mechanics* 415, pp. 117–153.

Wang, L.-P., O. Ayala, B. Rosa, and W. W. Grabowski (2008). "Turbulent collision efficiency of heavy particles relevant to cloud droplets". In: *New Journal of Physics* 10, 075013.

Wang, L.-P., B. Rosa, H. Gao, G. He, and G. Jin (2009). "Turbulent collision of inertial particles: Point-particle based, hybrid simulations and beyond". In: *International Journal of Multiphase Flow* 35, pp. 854–867.

Yang, C. Y. and U. Lei (1998). "The role of the turbulent scales in the settling velocity of heavy particles in homogeneous isotropic turbulence". In: *Journal of Fluid Mechanics* 371, pp. 179–205.

Yang, Y., G.-W. He, and L.-P. Wang (2008). "Effects of subgrid scale modelling on Lagrangian statistics in lagre-eddy simulation". In: *Journal of Turbulence* 9 (8), pp. 1–24.

Yavuz, M. A., R. P. J. Kunnen, G. J. F. van Heijst, and H. J. H. Clercx (2018). "Extreme Small-Scale Clustering of Droplets in Turbulence Driven by Hydrodynamic Interactions". In: *Physical Review Letters* 120 (24), pp. 179–205.

Zheng, J., P. Liu, and Z. Shen (2020). "Simulation of Turbulent Combustion in a Large Pulverized Coal Boiler Based on Turbulent Radiation Interaction and the Modified Soot Model". In: *ACS OMEGA* 5, pp. 23822–35.